Palaeogeography, Palaeoclimatology, Palaeoecology 671 (2025) 112977

Contents lists available at ScienceDirect

Palaeogeography, Palaeoclimatology, Palaeoecology

journal homepage: www.elsevier.com/locate/palaeo

Holocene palaeoclimatic evolution in the North Ionian Basin of the Mediterranean Sea: A multiproxy approach

L. Bronzo[a,b,c,*], A. Cascella[b], S. Bonomo[b,d], C. Morigi[c], I. Cacho[e], G. Margaritelli[f], J. Frigola[e], L.D. Pena[e], F. Lirer[g]

[a] *Università degli Studi di Firenze, Dipartimento di Scienze della Terra, Via Giorgio La Pira 4, 50121 Firenze, Italy*
[b] *Istituto Nazionale di Geofisica e Vulcanologia (INGV), Via Cesare Battisti 53, 56125 Pisa, Italy*
[c] *Università di Pisa, Dipartimento di Scienze della Terra, Via Santa Maria 53, 56126 Pisa, Italy*
[d] *CNR, Istituto di Geologia Ambientale e Geoingegneria (IGAG), Area Della Ricerca di Roma, 1, 00015 Montelibretti, Italy*
[e] *GRC Geociències Marines, Dept. de Dinàmica de la Terra i de l'Oceà, Facultat de Ciències de la Terra, Universitat de Barcelona, C/ Martí i Franqués s/n, 08028 Barcelona, Spain*
[f] *Dipartimento di Fisica e Geologia, Università degli Studi di Perugia, Via A. Pascoli, 06123 Perugia, Italy*
[g] *Sapienza Università di Roma, Dipartimento di Scienze della Terra, Piazzale Aldo Moro 5, 00185 Roma, Italy*

ARTICLE INFO

Editor: Howard Falcon-Lang

Keywords:
Calcareous nannoplankton
Wavelet analysis
Bond events
Rapid climate changes
North Atlantic Oscillation (NAO)

ABSTRACT

We analyse the ND14Mbis gravity core obtained from the North Ionian Basin using a multi-proxy approach (calcareous nannofossils, planktonic foraminifera, geochemistry, X-ray fluorescence), to improve knowledge of Holocene palaeoclimatic and palaeoceanographic evolution. Wavelet analysis of the cold water coccolith species group (*Emiliania huxleyi* > 4 μm and *Gephyrocapsa muellerae*) reveals a 1.6 ky periodicity, which closely matches the 1.5 ky North Atlantic Bond cycles. On shorter timescales, our high-resolution analysis allows the identification of major climatic events, including the latter part of the African Humid Period (10–5.4 ky BP) and the deposition of the Sapropel 1 interval (S1, 10–6.6 ky BP), as well as the Pre-Roman (4.1–2 ky BP), Roman (2–1.5 ky BP) and Post-Roman (1.5–0 ky BP) periods. During the African Humid Period, the S1 interval is clearly marked by the distribution of *Florisphaera profunda, Syracosphaera pulchra, Braarudosphaera bigelowii* and warm water taxa (*Calciosolenia* sp., *Discosphaera tubifera, Oolithotus fragilis, Rhabdosphaera clavigera, Umbilicosphaera* sp. and *Umbellosphaera tenuis*), reworked coccoliths and XRF signals. Our findings show that S1 anoxic bottom-water conditions were interrupted during two short spells of climate cooling that coincide with the 8.2 and 7.4 ky BP climate events. Drier conditions developed at the end of the African Humid Period, with intermittent humid intervals. These episodes were likely governed by the negative shifts of the North Atlantic Oscillation system, whose influence progressively intensified after 4.2 ky BP, as reflected by the oscillations in holococcolith abundance and K/Al curves.

1. Introduction

Thanks to its unique geographic position, the Mediterranean region plays an excellent role for investigating rapid climate variability during the Holocene. Being located in a transitional zone between North African and European climates, it is influenced by the interplay of several atmospheric systems, including tropical circulation cells (Azores high-pressure centre) and mid-latitude westerlies and cyclogenesis (Icelandic low-pressure centre) (Bolle, 2003; Tzedakis et al., 2009). Mediterranean precipitation patterns are strongly impacted by the interaction between these atmospheric systems, but also by the oscillatory phenomena acting from seasonal to decadal scales, such as the North Atlantic Oscillation (NAO) system, the variability of the African monsoon and global-scale climatic fluctuations such as El Niño Southern Oscillation (Wanner et al., 2001; Kalimeris et al., 2017 and references therein).

The Holocene (Walker et al., 2009) climatic variability in the Mediterranean has been extensively studied, revealing a complex nature driven by oscillations from centennial to millennial timescales (O'Brien et al., 1995; Rohling et al., 1995, 2009; Wanner et al., 2011). This period has been punctuated by several *quasi*-periodic rapid climatic changes (Mayewski et al., 2004) and modifications in hydrological features via

* Corresponding author at: Università degli Studi di Firenze, Dipartimento di Scienze della Terra, Via Giorgio La Pira 4, 50121 Firenze, Italy.
E-mail address: laura.bronzo@unifi.it (L. Bronzo).

https://doi.org/10.1016/j.palaeo.2025.112977
Received 21 January 2025; Received in revised form 15 April 2025; Accepted 23 April 2025
Available online 28 April 2025

freshwater inputs and/or enhanced evaporation that have been documented in different marine and continental archives (e.g. Rossignol-Strick et al., 1982; Rohling, 1994; Rohling and De Rijk, 1999; Duplessy et al., 2005; Finné et al., 2019 and references therein).

Globally, external factors such as solar irradiance oscillations (e.g. Van Geel et al., 1999; DeMenocal et al., 2000; Vonmoos et al., 2006; Shindell et al., 2020) and volcanic activity (e.g. Shindell et al., 2003; Wagner and Zorita, 2005; Kobashi et al., 2017), along with oceanic-triggered internal factors (e.g. Broecker, 2001; Debret et al., 2007, 2009; Sorrel et al., 2012), have been recognised as some of the main forcings of natural climate variability over the past 11.7 ky BP (e.g. rapid climate changes) (Mayewski et al., 2004). The overall Holocene Mediterranean climate variability passed through three main phases: a humid phase from the Early Holocene until 7.7 ky BP (Middle Holocene), an intermediate transitional period (Middle Holocene) from 7.7 to 5.5 ky BP, and arid conditions (Middle to Late Holocene) developed from 5.5 ky BP onwards (Magny et al., 2002, 2013; De Beaulieu et al., 2005; Frigola et al., 2007; Tzedakis et al., 2007; Sadori et al., 2008; Jalut et al., 2009; Vanniére et al., 2011; Siani et al., 2013). The first two phases correspond to the African Humid Period constrained approximately between 11.7 and 5.5 ky BP (Jolly et al., 1998; DeMenocal et al., 2000; Skonieczny et al., 2015) when an insolation-driven northward shift of the African tropical rain belt led to the formation of Sapropel 1 (S1) anoxic layer in the Eastern Mediterranean between approximately c.a. 10 and 6 cal. ky BP (e.g. Ritchie et al., 1985; Gasse, 2000; De Lange et al., 2008; Hennekam et al., 2014). This general pattern is superimposed on the timing of Holocene shorter climate change events (e.g. O'Brien et al., 1995; Bond et al., 2001; Rohling et al., 2002; Mayewski et al., 2004 among others). In particular, the 1.5 ky cycle of climate variability recognised in the North Atlantic region by Bond et al. (2001), has been addressed to major millennial scale warm/cold and humid/arid climate shifts in the Mediterranean and European regions (Desprat et al., 2013; Magny et al., 2013; Margaritelli et al., 2016; Di Rita et al., 2019). Over the last c.a. 5 ky BP, the recent literature highlighted that such short-term climate oscillations were documented in the Mediterranean, and could be chronologically correlated with the major archaeological subdivisions (Roberts et al., 2011; Lirer et al., 2014, 2019; Cisneros et al., 2016; Margaritelli et al., 2016, 2018, 2020) namely the Bronze Age, Iron Age, Roman Period, Late Antique Little Ice Age, Medieval Climate Anomaly and Little Ice Age.

The study of calcareous nannofossil assemblages has been proven to be a valuable tool for reconstructing Holocene paleoclimatic events in the Mediterranean Basin (e.g. Negri and Giunta, 2001; Sprovieri et al., 2003; Triantaphyllou et al., 2016; Cascella et al., 2019). The ecological preferences of living coccolithophores allow for investigating paleoclimatic changes, including vertical water column dynamics, sea surface temperature and total solar irradiance variations (Flores et al., 1997; Ausín et al., 2015; Incarbona et al., 2023). Furthermore, calcareous nannofossils redeposited in younger layers (i.e. reworked coccoliths) offer insights into sediment transport (e.g. Negri et al., 1999; Ferreira et al., 2008) and can be used to reconstruct regional-scale runoff and precipitation changes (e.g. Bonomo et al., 2014, 2016).

To contribute to a better understanding of Holocene paleoclimate changes in the Central Mediterranean area, this work presents new data from the sediment core ND14Mbis collected in the North Ionian Basin. We employed a multiproxy approach combining micropaleontological and geochemical analyses (including isotopic and XRF core scanner data) to investigate the causes of paleoclimatic variability on millennial to secular timescales. The newly generated dataset includes calcareous nannofossil assemblages and $\delta^{18}O_{Globigerinoides\ ruber\ \mathrm{white}}$ signal covering from 6 ky BP to the top of the core, along with $\delta^{13}C_{G.\ ruber\ \mathrm{white}}$ isotopic data and XRF-derived elemental ratios (Ca/Al, K/Al) for the entire studied interval. These results were integrated with previously published datasets, including planktic foraminifera (Checa et al., 2020), calcareous nannofossil abundances (Cascella et al., 2021), XRF Mn/Al and $\delta^{18}O_{G.\ ruber\ \mathrm{white}}$ isotopic signal (Checa et al., 2020) from the base of the studied interval up to 6 ky BP. Lastly, we provided wavelet analysis to investigate the principal periodicities documented in selected calcareous nannofossil group, aiming to understand if the Holocene climate system over the North Ionian Sea is linked to well-known regional to global cyclicities.

1.1. Modern oceanographic setting

The study site is located in a strategic area in which the water mass exchange between Western and Eastern Mediterranean basins, as well as between Adriatic and Ionian Seas, affects the water column at several depths (Fig. 1). From the Western Mediterranean Sea, the relatively fresher (c.a. 38.5 ‰) and cold surface Modified Atlantic Water (MAW) (core depth 100–200 m bsl) (Fig. 1a) crosses the Sicilian Channel into the Ionian Basin, occasionally branching northward into the Southern Adriatic Sea (Civitarese et al., 2010; Gacic et al., 2010). From the Eastern Mediterranean Sea, the warmer, saltier (c.a. 39 ‰) and deeper (c.a. 200–600 m bsl) Levantine Intermediate Water (LIW) (Fig. 1a) enters the Adriatic Sea through the Otranto Strait, where it mixes with cold and less saline waters formed by the winter cooling of North Adriatic shelf waters (Özsoy et al., 1989). This interaction results in the formation of the Adriatic Deep Water (ADW), which outflows through the Otranto Strait into the Northern Ionian Sea, settling below the LIW (Figs. 1a, c) and forming one of the principal components of the Eastern Mediterranean deep water (Manca et al., 2003; Theocharis et al., 2014). In the Adriatic Sea, shallow low-salinity waters form as a result of the Po River discharge (Özsoy et al., 1989). These fresher waters are transported southward by the Western Adriatic Current (WAC) into the Northern Ionian Sea, where they flow above the saltier MAW layer (Figs. 1a, c) (Turchetto et al., 2007; Bignami et al., 2007). The WAC is characterised by marked seasonality, with significantly stronger flow during the winter months (Milligan and Cattaneo, 2007).

The water mass dynamics in the Northern Ionian Sea are further affected by the Northern Ionian Gyre (NIG), which undergoes *quasi*-decadal reversals between cyclonic and anticyclonic modes (Lavigne et al., 2018). These shifts significantly impact the chemical and physical properties of the water column. In particular, during NIG cyclonic mode the influx of saltier and warmer LIW into the Southern Adriatic Basin promotes deep convection and the formation of denser ADW. Conversely, during anticyclonic NIG mode, the inflow of fresher and colder MAW into the Southern Adriatic Basin fosters the formation of lower-density ADW (Civitarese et al., 2010). This variability has been linked to pressure and wind-driven patterns over the Ionian Basin (Molcard et al., 2002; Pinardi et al., 2015) or by the ADW formation phases, known as the Adriatic Ionian Bimodal Oscillating System (BiOS) (Borzelli et al., 2009; Civitarese et al., 2010). From an ecological perspective, the NIG oscillations regulate the nutricline position, leading to two distinct trophic regimes. During NIG cyclonic regime more eutrophic conditions develop characterised by a deeper nutricline and by the occurrence of nutrient-rich waters, favouring phytoplankton bloom during spring. Conversely, during anticyclonic NIG phase more oligotrophic conditions develop with a shallower nutricline and recycled nutrients, preventing a prominent phytoplankton bloom (Civitarese et al., 2010; Lavigne et al., 2018).

2. Material and methods

2.1. Sediment core

The ND14Mbis gravity core was recovered at a water depth of 655 m in the northeastern part of the Ionian Sea (39°35′53,94"N, 18°47′40,48″E) (Fig. 1a) during the NEXTDATA2014 oceanographic cruise aboard the CNR R/V Urania. The total length of the core (332 cm) is characterised by greyish hemipelagic sediments. Two dark layers of 11 and 5 cm, interbedded by a light interval of 5 cm, highlight the occurrence of the organic matter enriched Sapropel 1 (S1) layer between 105

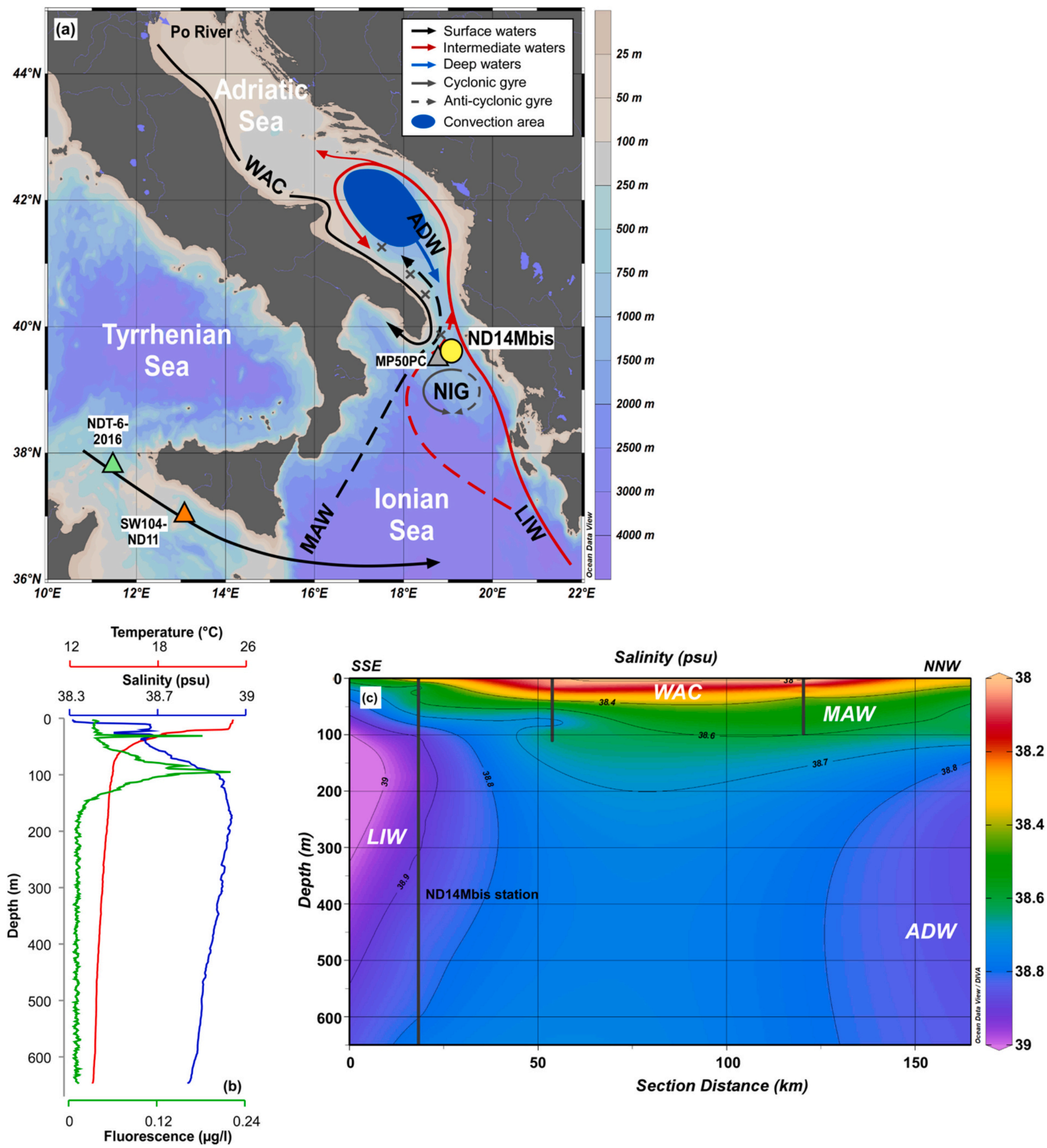

Fig. 1. a) Location of the ND14Mbis (yellow dot), NDT-6-2016 (green triangle) (Trias-Navarro et al., 2021), SW104-ND11 (orange triangle) (Margaritelli et al., 2020) and MP50PC (grey triangle) (Filippidi et al., 2016) sediment cores. The bathymetric map of the study area is overlayed with the main surface, intermediate, and deep circulation patterns. LIW: Levantine Intermediate Water, WAC: Western Adriatic Current, ADW: Adriatic Deep Water with its accumulation cell, MAW: Modified Atlantic Water. NIG: North Ionian Gyre, continuous lines represent the cyclonic circulation mode, dashed lines represent the anticyclonic mode of the BiOS: Bimodal Oscillating System (Civitarese et al., 2010). The blue arrow in North Eastern Italy evidences the Po River mouth. The grey crosses highlight a few sites where CTD profiles were acquired during the NEXTDATA 2014 cruise. b) Scatter plot of ND14Mbis station reporting Depth (0–650 m) against the CTD data (Temperature, Fluorescence, Salinity). c) Depth profile of water mass circulation on a transect acquired during NEXTDATA 2014 cruise in the SSE-NNW direction. On the *Z*-axis, the salinity value is plotted. The measurement logs are evidenced (dark vertical lines), and the ND14Mbis station is shown. (For interpretation of the references to colour in this figure legend, the reader is referred to the web version of this article.)

and 126 cm below the seafloor (bsf), already studied by Checa et al. (2020) and Cascella et al. (2021) (Fig. 2). In this work we have focussed on the stratigraphic interval between 0 and 132 cm bsf carrying a 1 cm resolution analysis. We adopted the Bayesian age model of Checa et al. (2020) (Fig. 2) based on ten radiocarbon (^{14}C) accelerated mass spectrometry (AMS) measurements and we studied the interval constrained between 0 and 10 ky BP.

2.2. Stable isotopes

$\delta^{18}O$ and $\delta^{13}C$ ratios were assessed on the planktonic foraminifera *Globigerinoides ruber* sensu stricto white variety at the University of Barcelona (CCiT-UB). For the $\delta^{18}O_{G.\ ruber\ \mathrm{white}}$ and $\delta^{13}C_{G.\ ruber\ \mathrm{white}}$, the analysis involved selecting 10 and 15 specimens from the >150 μm fraction, with a resolution of 1 cm, as detailed by Checa et al. (2020).

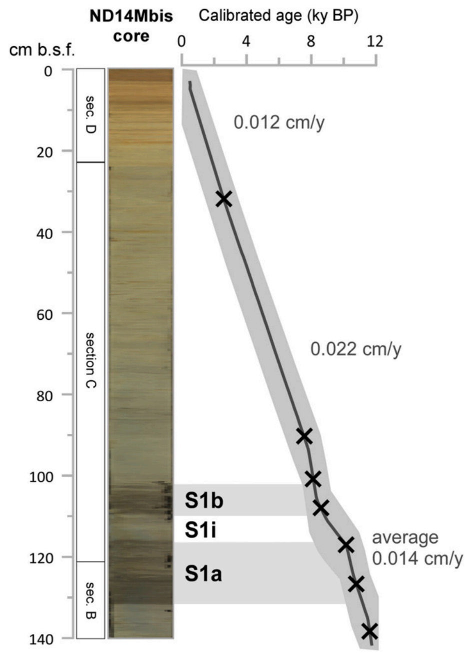

Fig. 2. High-resolution digital image, age model and sediment rates of the core ND14Mbis (from Checa et al., 2020). Age-depth correspondence is marked with the dark line, with crosses indicating the location of radiocarbon-dated samples; the light grey cloud represents age uncertainties (sigma 2). S1: Sapropel 1 (a, i – interruption, b phases).

The estimated external reproducibility was <0.05 ‰ and < 0.03 ‰ for $\delta^{18}O_{G.\ ruber\ \mathrm{white}}$ and $\delta^{13}C_{G.\ ruber\ \mathrm{white}}$, respectively. While Checa et al. (2020) previously analysed the $\delta^{18}O_{G.\ ruber\ \mathrm{white}}$ dataset for the interval between 11.5 and 6 ky BP, this study presents new $\delta^{18}O_{G.\ ruber\ \mathrm{white}}$ results from the upper portion (6–0 ky BP). The $\delta^{13}C_{G.\ ruber\ \mathrm{white}}$ data is newly presented here for the studied interval (10–0 ky BP).

2.3. Calcareous nannofossil assemblages

Calcareous nannofossil investigation was carried out on every centimetre of the ND14Mbis studied core, providing a temporal resolution of ca. 75 years per sample, according to the age model of Checa et al. (2020). Unprocessed sediments were prepared as smear slides (Bown, 1998) and observed at the transmitted light microscope at x1250 magnification. The relative abundance of in situ specimens expressed as percentages, was calculated over a total of 500 coccoliths per sample (average 6 fields of view) which allows a probability greater than 99 % of encountering a taxon whose abundance in the population is <1 % (Crow et al., 1960; Rio et al., 1990). Contemporarily, the abundance of reworked coccoliths ("reworked" hereafter) was evaluated, where their percentages were calculated from the sum of the in situ plus reworked. In general, the identification of the species follows the taxonomic criteria of Young et al. (2003) and Jordan et al. (2004). As for the identification of *Emiliania huxleyi* large (>4 μm) morphotype, we follow Flores et al. (2010). According to their ecological and morphological affinities, some taxa were grouped as follows: warm water group including *Calciosolenia* sp., *Discosphaera tubifera, Oolithotus fragilis, Rhabdosphaera clavigera, Umbilicosphaera* sp. and *Umbellosphaera tenuis;* cold water group including *E. huxleyi* large and *Gephyrocapsa muellerae*; the holococcoliths group comprises haploid lifecycle phases of *Calcidiscus leptoporus* (*C. leptoporus* subsp. *quadriperforatus* HOL), *Helicosphaera carteri* (*H. carteri catilliferus* type, *H. carteri* HOL *confusus* type) and *Syracosphaera pulchra* (*S. pulchra* HOL *oblonga* type, *S. pulchra* HOL *pirus* type) taxa; lastly, the placoliths group includes *E. huxleyi* < 4 μm and *E. huxleyi* large, *G. muellerae*, *G. oceanica*, *G. caribbeanica* and small *Gephyrocapsa* (<3 μm) (Incarbona et al., 2010; Di Stefano and Incarbona, 2004; Bonomo et al., 2021).

2.4. Cluster analysis

Considering the ecological preferences of the counted calcareous nannofossil taxa, stratigraphic constrained cluster analysis was performed on the total associations of in situ species, excluding reworked specimens. To eliminate redundant data and ensure good-quality clusters, the abundances of singular species were normalised by subtracting the mean and dividing by the standard deviation. With this approach, the abundances of the singular species contribute equally to the analysis, preventing any single taxon with very high or low values from dominating the clustering process (Wu et al., 2007). The analysis was conducted with the R software (version 4.0.1) using the "rioja" package (Juggins, 2015 – version 1.0–5).

2.5. Spectral analysis

The Ensemble Empirical Mode Decomposition algorithm (EEMD) (Wu and Huang, 2011) was used to examine the cold water calcareous nannofossil group signal to highlight possible non-linear and non-stationary frequency changes over time. The EEMD is an adaptive noise-assisted data analysis method that enhances the Empirical Mode Decomposition (EMD) by Huang et al. (1998).

This algorithm facilitates the dissection of a given time series data, identifying and separating short time-scale events from a prevalent trend. The underlying principle of this robust investigative approach relies on the assumption that any intricate signal can be broken down into a finite, often small, number of components referred to as "Intrinsic Mode Functions" (IMFs) (Huang et al., 1998). Each IMF can emphasise the inherent characteristics of simple oscillation occurring on a distinct timescale. For IMF components analysis, the "REDFIT "and Cross-wavelet Transform (XWT) methods were applied, involving the linear detrending of all data before analysis. The analyses were conducted using R (version 4.0.1) along with the Rlibeemd (Luukko et al., 2016), drip (Bunn, 2010) and WaveletComp (Roesch and Schmidbauer, 2018) packages.

2.6. X-Ray Fluorescence (XRF)

Bulk elemental geochemical parameters were used to understand some aspects of climatically driven variations in sediment composition. The acquisition of sediment data was pursued through the Avaatech XRF core scanner at the CORELAB laboratory of the University of Barcelona. For detailed information, including the variations in barium (Ba)/aluminium (Al), sulfur (S)/Al, and manganese (Mn)/Al geochemical ratios between 11.5 and 6 ky BP, see Checa et al. (2020). In this study, we focussed instead on the geochemical elemental ratios calcium (Ca)/titanium (Ti) and potassium (K)/Al for the interval between 10 and 0 ky BP.

In particular, the Ca/Ti ratio was considered to evaluate the degree of carbonate dilution in the analysed record (Rincón-Martínez et al., 2010). The Ca is conventionally interpreted as a measure of biogenic production (e.g. Cheshire et al., 2005; Solignac et al., 2011), while Ti is a proxy of terrigenous input. In the nearby Apulian margin, where sediments enriched in carbonates are depleted in clay minerals, the Ca/Ti ratio becomes a valuable proxy for tracing fluctuations in the relative abundance of marine biogenic carbonate and terrestrial input (e.g. Richter et al., 2006; Rothwell and Rack, 2006; Goudeau et al., 2015). The K/Al ratio was taken into account as a supplementary proxy for detrital riverine discharge, as K serves as an indicator of illite supply in sediments from Northern Mediterranean regions (Frigola et al., 2008; Nieto-Moreno et al., 2011; Martinez-Ruiz et al., 2015), it was normalised to Al in order to minimise the dilution effect (Calvert and Pedersen, 2007). All the ratios were calculated and expressed on a logarithmic scale (Weltje and Tjallingii, 2008).

3. Ecological preferences of calcareous nannofossil taxa and groups

In the Mediterranean area, the species constituting the placoliths group are considered r-strategy taxa capable of responding quickly to changes in trophic and environmental conditions. They are generally more abundant in temperate-cold mixed surface waters but also live in stable and stratified waters (Knappertsbusch, 1993; Ziveri and Thunell, 2000). Instead, the *E. huxleyi* larger morphotype prefers cold water masses, sensibly reducing its abundance at the onset of the Holocene in the Mediterranean Sea (Colmenero-Hidalgo et al., 2002, 2004; Flores et al., 2010). Nevertheless, it has been recorded in the Western (Incarbona et al., 2023) and Central (Ferraro et al., 2018) Mediterranean marine sediments during this interval. *Gephyrocapsa muellerae* is another indicator of cold-water conditions as it was related to glacial periods in the Mediterranean Sea (Amore et al., 2004; Bazzicalupo et al., 2022). These two species, herein grouped in the cold water group, are also both associated with cold and fresher waters (e.g. Argenio et al., 2024 and references therein).

The warm water group consists of k-strategist taxa with a tropical/sub-tropical affinity, preferring warm and oligotrophic surface waters (Okada and McIntyre, 1977; Flores et al., 1999; Triantaphyllou et al., 2004; Dimiza et al., 2008; Oviedo et al., 2015; Bonomo et al., 2021). Similarly, holococcoliths show a preference for warm, oligotrophic stratified surface waters (Kleijne, 1991; Oviedo et al., 2015; D'Amario et al., 2017), exhibiting uniform behaviour despite belonging to different species (Oviedo et al., 2015). On the other hand, their relatively high abundance in the sediments has been used as a proxy of bottom-sea ventilation during cold periods (Roth and Coulbourn, 1982; Cascella et al., 2021; Incarbona et al., 2022).

The taxa *Florisphaera profunda, Gladiolithus flabellatus* and *Algirosphaera robusta* thrive under lower light conditions and high nutrient fluxes in the proximity of the thermocline base (Knappertsbusch, 1993; Malinverno et al., 2003; Triantaphyllou et al., 2004). *Florisphaera profunda,* which generally is the most abundant species of the lower photic taxa, has been widely used to monitor past changes in nutricline-depth and induced changes in surface coccolith productivity (Ausín et al., 2015; Tangunan et al., 2017; Incarbona et al., 2023). Considering the living coccolithophore communities of the Central Mediterranean, *F. profunda* is linked with deep (~75 to 200 m), relatively salty waters and a developed Deep Chlorophyll Maximum (DCM) (Bonomo et al., 2021). In the fossil marine archives, its relative abundance is higher in concomitance with the development of deep nutricline, responding to conditions of stable, stratified, oligotrophic surface waters during warmer climatic intervals (Triantaphyllou et al., 2009; Incarbona et al., 2010; Oviedo et al., 2015; Athanasiou et al., 2017; Bonomo et al., 2021; Skampa et al., 2024 and references therein).

Preferring conditions in which a DCM occurs, the species *Syracosphaera pulchra* shows relatively higher abundances within oligotrophic stratified waters (Ziveri and Thunell, 2000; Ziveri et al., 2004; Triantaphyllou et al., 2004; Bonomo et al., 2017; Crudeli et al., 2023). Particularly, this taxon is indicative of warmer surface waters and low salinity conditions, being locally associated with intervals characterised by precipitation maxima (Flores et al., 1997; Colmenero-Hidalgo et al., 2004; Ziveri et al., 2004; Dimiza et al., 2008, 2015; Malinverno et al., 2009, 2014; Karatsolis et al., 2017; Skampa et al., 2020). The taxon *Braarudosphaera bigelowii* has been also considered as an indicator of low salinity and high turbidity conditions associated with the release of riverine material (Bukry, 1973; Roth, 1994; Negri et al., 1999; Negri and Giunta, 2001; Principato et al., 2003; Triantaphyllou et al., 2004) and in the same core has been used to highlight the development of S1 conditions within the water column (Cascella et al., 2021).

4. Results

4.1. Calcareous nannofossils assemblages

In this section, we will present the distribution of the most significant taxa that were used for the paleoclimatic and paleoceanographic reconstruction of the last 10 ky at the study site (Fig. 3). Calcareous nannofossils are abundant and well preserved throughout the core. The placoliths group dominated the entire assemblage with mean values of c. a. 70 % (supplementary material). The taxon *F. profunda* is well represented in the assemblage. Its abundance decreases from the highest values at the onset of the S1 (29 %) until c.a. 7.5 ky BP, then it stabilises

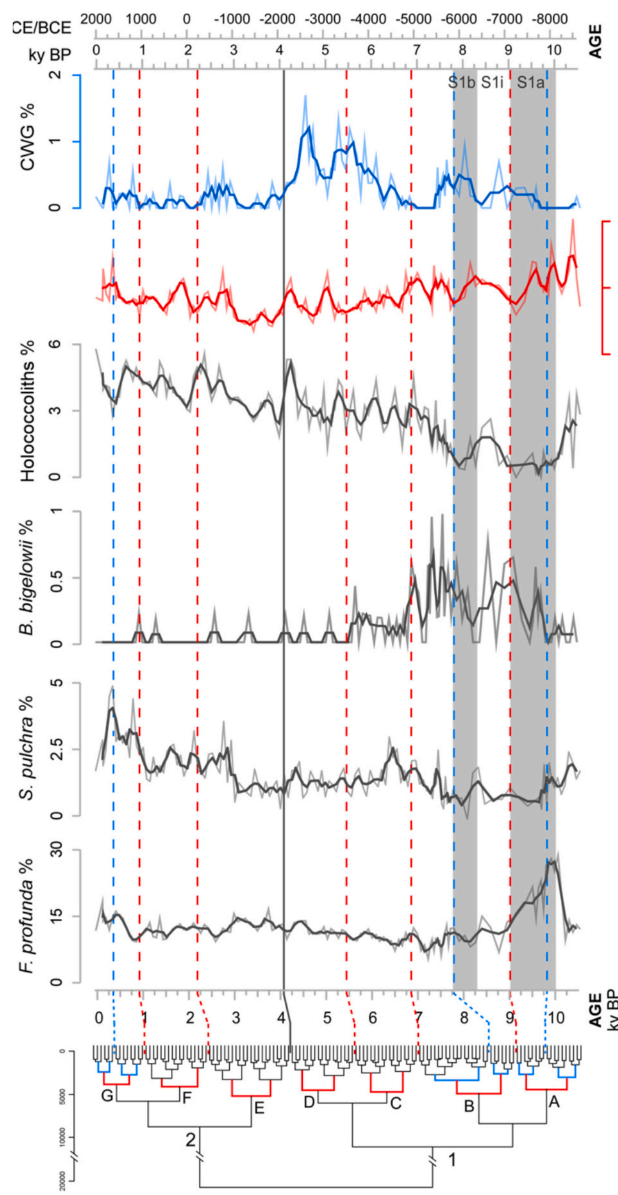

Fig. 3. Downcore variations of the discussed calcareous nannofossil taxa (%) plotted versus age for the ND14Mbis. Thicker lines represent the 3-point running average. The cluster dendrogram is also plotted against age. The dark straight line highlights the main break (clusters 1 and 2). Dashed red and blue lines represent subcluster groups (from A to G red dendrograms) and the secondary subdivisions (blue dendrograms). WWG: Warm Water Group, CWG: Cold Water Group. The grey bands represent the Sapropel 1 layer (S1 - a, b divisions), according to Checa et al. (2020) and Cascella et al. (2021). (For interpretation of the references to colour in this figure legend, the reader is referred to the web version of this article.)

around 11.45 % and increases again from c.a. 0.6 ky BP (Fig. 3). Other species, such as *C. leptoporus*, *H. carteri*, and *Syracosphaera mediterranea*, as well as those considered individually within both warm water (i.e., *U. tenuis*, *D. tubifera*, *O. fragilis*) and cold water (*G. muellerae*, *E. huxleyi* large) groups, are characterised by lower mean abundances (< 5 %) (supplementary material). *Syracosphaera pulchra* (Fig. 3) shows minimum average abundances (c.a. 1 %) within the S1 interval. From 7.7 ky BP, abundance fluctuations are recorded around mean values of 1.7 %, and finally, an increasing trend is recorded from c.a. 3 ky BP, peaking at c.a. 0.3 ky BP (4.7 %). *Braarudosphaera bigelowii* shows relatively higher values between 10 and 5.5 ky BP, reaching its maximum (0.9 %) at c.a. 7.6 ky BP. Afterwards, it decreases prominently, displaying low abundances towards the top of the core, almost disappearing (Fig. 3).

The holococcoliths show their lowest occurrence in the S1 layers, with a significant peak during the interruption phase (S1i, Fig. 3). From the end of S1, the curve follows a generally increasing trend, reaching their highest abundance (5.8 %) at the top of the core. The warm water group shows mean values of c.a. 4 % (Fig. 3). From the maximum (10.2 %) at the bottom of the study record (10.4 ky BP), the curve follows a decreasing trend until c.a. 3.5 ky BP. Afterwards, the values increase again, oscillating around a mean of 5 %. The cold water group displays abundances <2 % with an average value of 0.3 %. More abundant values are displayed between 7 ky BP and 4 ky BP, reaching two peaks at c.a. 5.3 ky BP (1.3 %) and at c.a. 4.5 ky BP (1.7 %).

4.2. Clusters

The clustering evidence two major groups (1 and 2) developing from the main dendrogram which breaks at c.a. 4.1 ky BP (Fig. 3). This principal subdivision highlights a general modification in the calcareous nannofossil assemblages due to a sharp reduction of the species *E. huxleyi* large and *G. muellerae* (supplementary material). Group 1 is characterised by four subgroups, which define the intervals from the bottom of the core to 9 ky BP (cluster A), 9 to 6.8 ky BP (cluster B), 6.8 to 5.4 (Cluster C), and 5.4 to 4.1 ky BP (cluster D). Group 2 is subdivided into three subgroups from 4.1 to 2.2 ky BP (cluster E), 2.2 to 0.9 ky BP (cluster F) and lastly, from 0.9 ky BP until the top of the core (cluster G). In general, clusters A and B are characterised by higher values of *F. profunda* and *B. bigelowii* and lower abundances of *S. pulchra* and holococcoliths, highlighting the principal features of the S1 interval (Checa et al., 2020; Cascella et al., 2021). In particular, the two subclusters centred at c.a. 9.8 ky BP and 7.7 ky BP for clusters A and B respectively (Fig. 3), evidence the onset and the end of the S1 layer according to the time intervals described for the same core by Checa et al. (2020) and Cascella et al. (2021).

4.3. Reworked coccoliths and XRF

The relative abundance of reworked coccoliths displays some peculiar oscillations throughout the interval, of which the most remarkable ones are located in the S1 layer. In particular, within the S1 episode, reworked relative peaks are centred at 9.6 ky BP (30.6 %), 8.6 ky BP (28.5 %) and 7.7 ky BP (31.6 %), alternated by relative minima of about 19 % centred at 9.1 ky BP and 8.1 ky BP (Fig. 4). Reworked maximum (31.6 %) is reached at the end of S1 (7.7 ky BP). Afterwards, the curve sharply drops to a relative minimum (8.2 %) at 6.2 ky BP (Fig. 4). Between 6.2 and 2.3 ky BP, the reworked trend slightly decreases, displaying mean abundances of 11.6 %. Lastly, from 2.3 ky BP up to the top of the core, the values increase again from 4.5 % to 15 % (Fig. 4).

XRF elemental ratios evidence several fluctuations. In particular, the K/Al ratio generally shows decreasing values from 10 to c.a. 2.3 ky BP, increasing towards the top of the core. However, the curve displays several high amplitude fluctuations superimposed on the general trend (Fig. 4). High values are observed at around 10–7.7 ky BP, 6.8–5.5 ky BP, 4.2–3.5 ky BP, 3–2.3 ky BP and lastly from 1.2 ky BP until the upper part of the core (Fig. 4). The Ca/Ti ratio instead, shows a progressive decreasing pattern characterised by four intervals of lower values between 7 and 6 ky BP, 4.3–3.9 ky BP, 2.7–2.3 ky BP and 0.5–0 ky BP, and slightly increased ratio between 2.3 and 0.5 ky BP (Fig. 4).

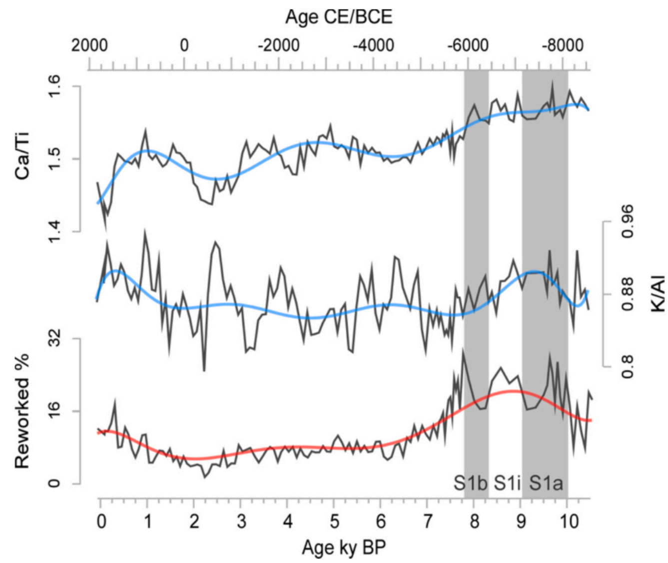

Fig. 4. Reworked relative abundance (%), logarithmic Ca/Ti and K/Al ratios are plotted versus age for ND14Mbis core. Smoothed trends are represented by orthogonal polynomial interpolations with a 7th-degree for the reworked curve, 10th-degree for the K/Al ratio, and 9th-degree for the Ca/Ti ratio.

4.4. Stable isotopes

The $\delta^{13}C_{G.\ ruber\ white}$ exhibits lighter isotopic ratios between 10 and 6.3 ky BP (Fig. 5), with values fluctuating around 0.2 ‰. Notably, a shift towards heavier values (1 ‰) around 7.4 ky BP and another towards lighter values (−0.32 ‰) around 6.4 ky BP occur. From 6.3 ky BP onward, the values stabilise around 1.2 ‰, showing some minor fluctuations. The curve drops again at c.a. 2.7 ky BP (0.9 ‰), with isotopic ratios shifting around 1 ‰ until 1.8 ky BP, where lower values are reached once again (0.4 ‰). Towards the top of the core, the ratio oscillates around 0.8 ‰ and slightly negative values (−0.1 ‰) are observed at 0 ky BP (Fig. 5).

Lower $\delta^{18}O_{G.\ ruber\ white}$ values (c.a. 0.1 ‰) were recorded between 10

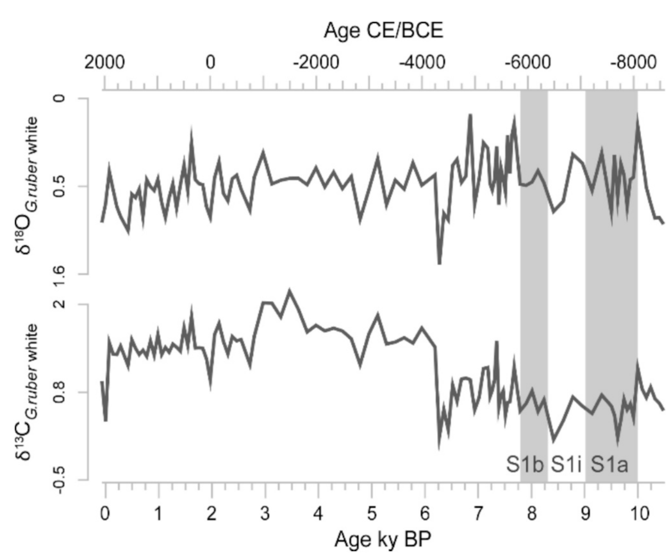

Fig. 5. Isotopic data of $\delta^{13}C_{G.ruber\ white}$ and $\delta^{18}O_{G.ruber\ white}$ of core ND14Mbis plotted against age ky BP.

and 6.5 ky BP. However, heavier values are observed around 8.5 ky BP, where the isotopic ratio registers 0.7 ‰ (Fig. 5). Around 6.4 ky BP, the heaviest ratio is shown, with the curve dropping towards 1.4 ‰. Afterwards, the $\delta^{18}O_{G.\ ruber\ \mathrm{white}}$ settles around 0.5 ‰, reaching heavier ratios at c.a. 4.5, 2.5, 2 and 0.5 ky BP. Between 6.3 ky BP and the top of the record, the lowest value (0.3 ‰) is recorded at c.a. 1.8 ky BP (Fig. 5).

4.5. Spectral analysis

The EEMD analysis carried out on the calcareous nannofossil cold water group revealed six IMF components. Among them, only the IMF3 component recorded a significant periodicity (Fig. 6) (supplementary material), while the other components recorded mainly noise (IMF1, 4, 5 and 6) and/or an unclear signal (IMF 2) (supplementary material). The component IMF3 and power spectral analysis, performed in the time domain, revealed prominent peaks at 1.6, 1.2 and 1.04 ky, above the 90 and 95 % Interval of Confidence (IC) (Fig. 6b). In particular, the wavelet analysis (Fig. 6b) indicates that the periodicity associated with 1.6 ky is clearly present on the studied record between 10 and 2.3 ky BP and becomes gradually weaker towards the top of the core (Fig. 6c).

5. Discussions: paleoenvironmental reconstruction in the North Ionian Sea

The dataset obtained from the ND14Mbis record was integrated with literature data (e.g., Bond et al., 2001; Lambeck et al., 2014; Smith et al., 2016; Checa et al., 2020) (Figs. 7, 8) to provide a detailed reconstruction of paleoclimatic events documented in the sedimentary archive. These events chronologically correspond to those described in Rohling et al. (2002) from 10 ky BP to c.a. 5 ky BP and Margaritelli et al. (2016) for the last five millennia. Since the S1 interval has been thoroughly investigated by Checa et al. (2020) and Cascella et al. (2021), the discussion will primarily focus on the period between 7.7 and 0 ky BP, with particular attention to the termination of the S1 episode.

Furthermore, following the approach proposed by Bonomo et al. (2016) and Cascella et al. (2019), variations in reworked coccoliths and calcareous nannofossil abundances were discussed along with the NAO index (Smith et al., 2016) and compared with XRF values (reversed Ca/

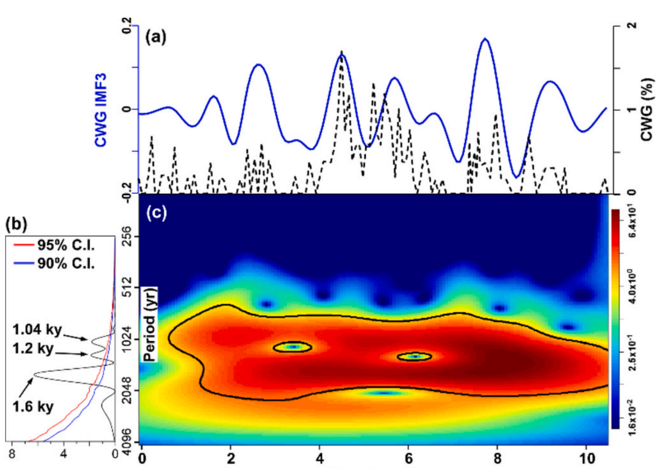

Fig. 6. Cold water group (CWG) signal analysis displayed in the time domain. In (a) is shown the comparison between the IMF3 and the abundance of CWG (%). The IMF3 periodogram (b) and continuous wavelet transform power spectrum (c) are displayed. In the periodogram (b), significant periodicity and relative values (expressed in ky) are reported, with the red and blue lines representing the 95 % and 90 % confidence levels, respectively. The black lines in (c) represent the 90 % confidence level. (For interpretation of the references to colour in this figure legend, the reader is referred to the web version of this article.)

Ti trend, K/Al) (Fig. 7). In general, the NAO-like oscillatory system is suggested to have influenced the Mediterranean climate, at least over the past six millennia (Fletcher et al., 2013), modulating long-term trends in temperature and precipitation across the Italian peninsula (e.g., Cascella et al., 2019, and references therein). In the Central Mediterranean, positive NAO conditions are associated with colder and drier winters, while negative NAO phases correspond to warmer and wetter winters (López-Moreno et al., 2011; Benito et al., 2015). This mechanism has been primarily attributed to variations in the intensity and direction of the westerlies and the related hydroclimatic cycle of the Mediterranean (Marshall et al., 2002; Giraudi, 2011; Fletcher et al., 2013). In particular, under negative NAO conditions, a weakened westerly flow causes Atlantic winter storm tracks to converge over Central-Western Europe, resulting in maximum winter rainfall (e.g. Zielhofer et al., 2017).

In general, NAO fluctuations to some extent have also been suggested to have influenced the development of the North Atlantic Bond events (Margaritelli et al., 2016 and references therein), which also in Europe and the Mediterranean areas have been detected with 1.5 ky cyclicities characterised by shifts between warm/cold and humid/arid climatic conditions (Desprat et al., 2013; Magny et al., 2013; Margaritelli et al., 2016). This aspect was investigated by conducting a spectral analysis on the cold water group IMF3 signal, which revealed a 1.6 ky periodicity. The results were then compared with the Hematite-Stained Grains (HSG) curve (Bond et al., 2001), showing oscillations comparable to the 1.5 ky Bond cyclicities. Overall, the climate at the study site over the past 10 ky appears to have been dominated by oscillations between warmer and cooler/drier conditions, investigating such fluctuations in relation to underlying oscillatory climatic mechanisms.

5.1. African humid period (10–5.4 ky BP)

The most recent African Humid Period (11.7–5.5 ky BP) (Skonieczny et al., 2015) was associated with increased precipitation in Northern and Western Africa due to a northward migration of the tropical rain belt, which led to a stronger West African Monsoon, linked to changes in solar irradiance and albedo feedback (e.g. Jolly et al., 1998; DeMenocal et al., 2000; Burrough and Thomas., 2013; Skonieczny et al., 2015), also driving increased moisture import towards the Mediterranean basin (Vermeersch, 2008). The stronger precipitation in Northern and Western Africa enhanced Nile River discharge leading to changes in sediment patterns (e.g. Muhs, 2013) and increased marine food web productivity in the Mediterranean Sea, driving the deposition of S1 layer between c.a. 10 and 6 ky BP (Rohling et al., 2015; Casford et al., 2002, 2003; De Lange et al., 2008; Geraga et al., 2008; Triantaphyllou et al., 2009, 2014, 2016; Siani et al., 2010; Filippidi et al., 2016; Tesi et al., 2017; Filippidi and De Lange, 2019). In the studied ND14Mbis record, the S1, with its internal subdivisions (S1a, S1i, S1b), was identified and analysed by Checa et al. (2020) and Cascella et al. (2021) through planktonic foraminifer, calcareous nannofossil quantitative investigation and XRF proxy records. During the S1a phase (10–9 ky BP) (Fig. 8), planktonic foraminifera and calcareous nannofossils documented water column stratification and strong reduction of bottom water ventilation, linked to warm and oligotrophic conditions (Checa et al., 2020; Cascella et al., 2021) and associated with enhanced continental runoff (Cascella et al., 2021). The S1a phase is followed upwards by a short time interval (interruption of S1 - S1i phase, 9–8.2 ky BP, Fig. 8) during which a brief production of colder waters caused mixing of the stratified water column and re-ventilation of the deep dysoxic waters (Checa et al., 2020). A third phase, similar to S1a developed (S1b, 8.2–7.7 ky BP, Fig. 8), characterised by warm and oligotrophic conditions (Checa et al., 2020), but with less productivity and weaker water column stratification that caused less dysoxic deep waters. The Mn marker layer recorded in the studied core at c.a. 7.7 ky BP (Fig. 8) geochemically identifies the demise of the S1 layer (Checa et al., 2020), indicating the re-oxygenation of dysoxic bottom waters (e.g., Martinez-Ruiz et al., 2000; Meier et al.,

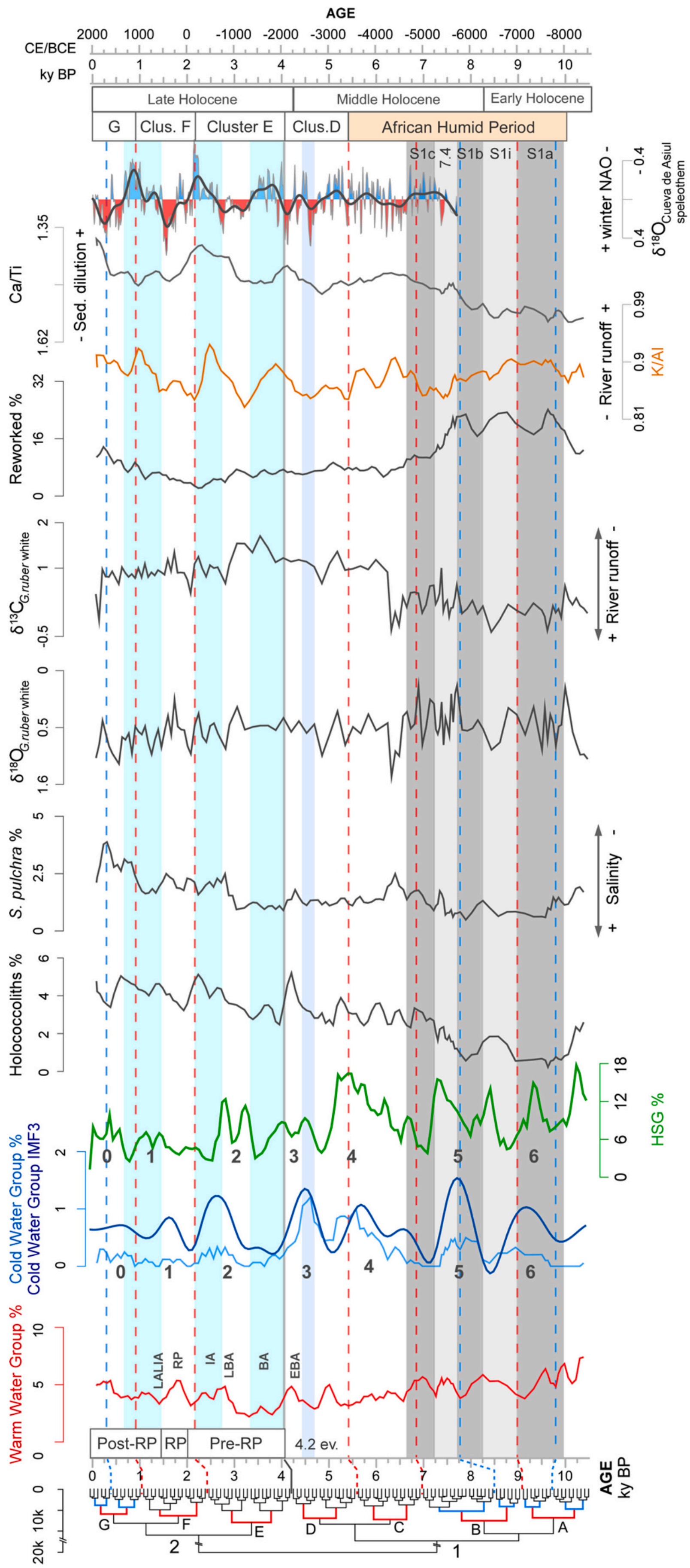

(caption on next page)

Fig. 7. Downcore variations of selected coccolith taxa (%, 3 points running average) are plotted versus age (ky BP, Before Current Era – BCE and Current Era – CE) for ND14Mbis core. The cold water group IMF3 is shown with the numbers of Bond events (6 to 0) associated with those of the Hematite Stained Grain (HSG %) curve by Bond et al. (2001). The cluster dendrogram and its subdivisions (A to G) are displayed and limited by the continuous and dashed lines: dark for the main dendrogram subdivision and red and blue for the subclusters. Coccolith abundance is compared with $\delta^{18}O_{G.ruber\ white}$ and $\delta^{13}C_{G.ruber\ white}$ stable isotopes, XRF (Ca/Ti curve reversed, and K/Al) data. The climatic episodes EBA: Early Bronze Age, BA: Bronze Age, LBA: Late Bronze Age, IA: Iron Age, RP: Roman Period, LALIA: Late Antique Little Ice Age are based on Margaritelli et al. (2016, 2020). The North Atlantic Oscillation (NAO) reconstruction based on the Cueva de Asiul stalagmite $\delta^{18}O$ isotopic dataset (Smith et al., 2016) is displayed. The light blue bands represent the NAO negative prominent oscillations. (For interpretation of the references to colour in this figure legend, the reader is referred to the web version of this article.)

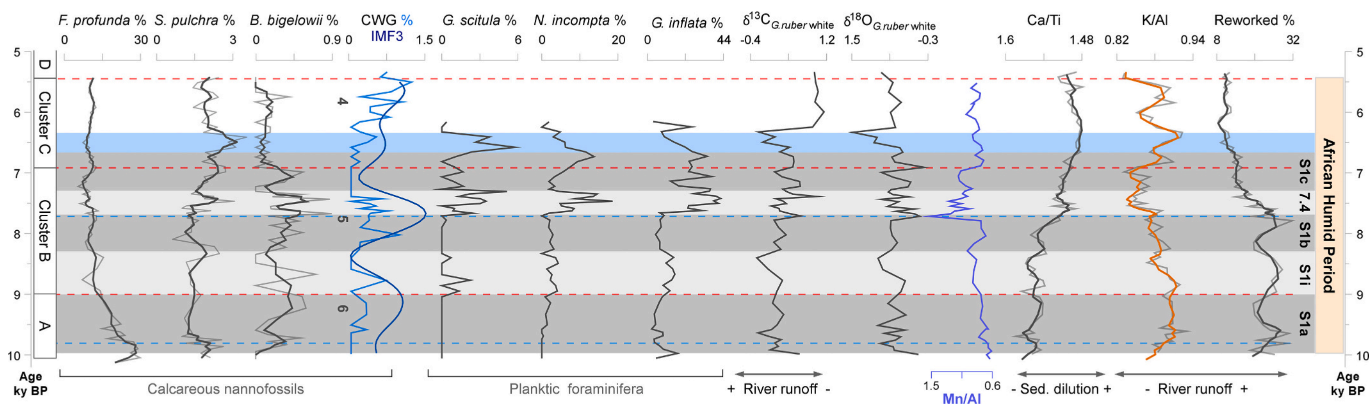

Fig. 8. Focus on the African Humid Period interval (10–5.4 ky BP), including S1a, S1i, and Sib subdivisions described by Checa et al. (2020) and Cascella et al. (2021) and the S1c subdivision discussed in this work. Calcareous nannofossil relative abundances (%, bulk and 3 points running average – thicker line), planktic foraminifera data and the Mn/Al curve from Checa et al. (2020), isotopic ($\delta^{18}O_{G.ruber\ white}$, $\delta^{13}C_{G.ruber\ white}$), and XRF data (Ca/Ti reversed curve, K/Al) are plotted against age. The cluster subdivision (A to D) is also highlighted with red dashed lines representing major cluster subdivisions and blue dashed lines representing secondary subdivisions. The cold water group (CWG) IMF3 curve is also plotted with indications of Bond events (6 to 4) (Bond et al., 2001). Darker grey bands represent stratification intervals, lighter grey bands indicate sapropel interruption intervals, and the blue band highlights enhanced Adriatic Deep Water outflow. (For interpretation of the references to colour in this figure legend, the reader is referred to the web version of this article.)

2004).

Nevertheless, the temporal framework of Cluster B, together with fluctuations in planktonic foraminifera and $\delta^{18}O_{G.\ ruber\ white}$ values (Fig. 8), suggests that sapropel-like conditions persisted until at least 6.8 ky BP, well beyond the end of the visible dark layer at 7.7 ky BP (Checa et al., 2020), as sustained by micropaleontological evidence. In particular, the calcareous planktonic assemblages suggest the renovation of sapropel-like conditions after a brief episode of climate cooling in the Eastern Mediterranean (Filippidi et al., 2016). Cool and mixing water conditions developed from 7.7 ky BP to 7.3 ky BP (Fig. 8). These features are evidenced by the increase of the calcareous nannofossils cold water group (CWG and IMF3 curves) and by heavier values in the $\delta^{18}O_{G.\ ruber\ white}$ signal (Fig. 8), associated with maxima abundances in planktonic foraminifera *Globorotalia scitula*, *G. inflata* and *Neogloboquadrina incompta*, indicating a well-developed thick and cold mixed layer (Pujol and Vergnaud Grazzini, 1995) (Fig. 8). Comparable conditions were observed in the planktic foraminifera assemblages in NDT-6-2016 core (Fig. 1a), where also a strong seasonality was indicated by high values of both *G. inflata* (winter mixing) and *G. ruber* (summer stratification). Such features have been linked to reduced water exchange at the Sicily Strait, sustained by the persistence of Eastern Mediterranean stagnation, the concomitant weakening of the eastward flow of Atlantic waters and the development of slightly cooler conditions (Trias-Navarro et al., 2021). Chronologically, the development of this new cool water condition coincides with the occurrence of the so-called “7.4 ky” cold event (Fig. 8) (e.g., Fletcher et al., 2010) and Bond Event 5 (Fig. 7). During this interval a decline in riverine runoff is recorded at our study site, as indicated by the decreasing trend in the reworked coccolith curve, associated with a shift in Ca/Ti and K/Al signatures (Fig. 8). These environmental conditions are well aligned with the millennial-scale variability of Nile River flooding linked to monsoon weakening due to reduced solar output (Finkel and Nichiizumi, 1997; Solanki et al., 2004). Prominent intervals of monsoon weakening were described from Levantine basin sediments around 9.3–8.8, 8.5–7.8 and 7.3–6.8 ky BP (Hennekam et al., 2014) and between 7.9 and 7.3 ky BP by Triantaphyllou et al. (2009), being also recorded in Central Mediterranean sediment records (Giunta et al., 2003; Sangiorgi et al., 2003; Filippidi et al., 2016; Incarbona and Sprovieri, 2020). During these short events, outbursts of cold northerly air masses reached the Mediterranean basin from Eastern European and Siberian sources (e.g. Rohling, 2000; Geraga et al., 2005; Gogou et al., 2007; Marino et al., 2009). Within this framework, a brief episode of partial reoxygenation of bottom waters, detected in an Adriatic-influenced sediment core, along with the more prominent resumption of deep water formation in the Aegean Sea, contributed to the formation of Mn-marker layers (Filippidi et al., 2016). Similarly, this process has also led to the formation of the Mn-marker layer at the studied core (Fig. 8) (Checa et al., 2020). According to our calcareous plankton data, we suggest a similitude with the S1i interruption event (8.2 ky BP, Checa et al., 2020; Cascella et al., 2021) (Fig. 8), also in agreement with Filippidi et al. (2016).

After the aforesaid cold and dry spell, relatively warmer and more stratified waters re-established between 7.3 and 6.6 ky BP, as evidenced by: i) the very low values of the calcareous nannofossil cold water group, the increasing trend of *S. pulchra*, the last peak of *B. bigelowii* and the slight increase of *F. profunda* values and ii) lighter values in the $\delta^{18}O_{G.\ ruber\ white}$, the increase in abundance of planktonic foraminifera warm water taxa (*G. ruber* white, *G. quadrilobatus*, *Orbulina universa*, from Checa et al., 2020) and the decrease in cold water ones (*G. scitula*, *N. incompta*) (Fig. 8). Nevertheless, *G. inflata* values remained relatively high (Fig. 8), indicating a gradual transition towards weaker stratification, likely associated with the development of a DCM, as also suggested by the slightly higher *F. profunda* values (Fig. 8). This pattern further implies the persistence of weak mixing conditions during winter (Trias-Navarro et al., 2021, and references therein). Such oscillations were also accompanied by higher release of continental material signals at the site as suggested by a small increment in the reworked coccoliths, in the K/

Al signal and by the shift in $\delta^{13}C_{G.\ ruber\ white}$ curve towards positive values. Generally, the values of planktic foraminifera carbon stable isotope $\delta^{13}C$ can be affected by various factors, such as the air-sea exchange of CO_2, photosynthesis-remineralisation cycle, surface water stratification (Rohling and Cooke, 1999), species-specific vital effects, symbiont activity (Spero, 1992), calcification depths in the mixed surface layer and thermocline (Mulitza et al., 1999), among others. However, in enclosed basins like the Mediterranean Sea, $\delta^{13}C$-based habitat reconstructions of planktic foraminifera may be biased by inputs of river runoff leading to decreased $\delta^{13}C$ values in epipelagic taxa and potential habitat changes (Rohling et al., 2004, 2015; Hennekam et al., 2014; Le Houedec et al., 2020). Considering the boundary conditions, the oscillations towards lower $\delta^{13}C_{G.\ ruber\ white}$ values in the studied record have been interpreted as an indication of the release of terrestrial organic matter via river runoff, notably ^{13}C-depleted (e.g. Mackensen and Schmiedl, 2019 and references therein).

These findings allowed us to propose a further subdivision of the S1 episode in the study area. Therefore, the S1c interval has been defined between 7.3 and 6.6 ky BP (Fig. 8), coeval with the final phase of the intermediate depth S1b (7.3–6.6 ky BP) described by Filippidi et al. (2016). This final phase was likely driven by the persistence of suboxic conditions, which sustained the prolonged development of S1 at the site, as observed in the Adriatic-influenced MP50PC sediment record (Filippidi et al., 2016). Differently, the intensified deep-water production in the Aegean Sea led to the formation of a more oxic S1 interval, as recorded in the KN3 sediment record (Filippidi et al., 2016). Nonetheless, these findings support the characterisation of a basin-wide framework of the S1 interval at intermediate depths under the influence of deep-water formation sites (Filippidi et al., 2016). The time interval between 6.8 and 5.4 ky BP (cluster C) covers the transition towards the demise of the African Humid Period influence (e.g. Filippidi and De Lange, 2019) (Fig. 8). Between 6.6 and 6.3 ky BP, the $\delta^{18}O_{G.\ ruber\ white}$ sharp shift towards heavier values (Fig. 8) evidences the resumption of ADW formation (Piva et al., 2008; Marino et al., 2009; Siani et al., 2013; Filippidi and De Lange, 2019; Incarbona and Sprovieri, 2020). Under such conditions, the *F. profunda* lower values, the progressively increasing trend of the calcareous nannofossil cold water group and peaks of planktonic foraminifera *G. scitula* associated with the presence of *G. inflata* and *N. incompta*, suggest the development of cold and maybe mixed waters (e.g. Pujol and Vergnaud Grazzini, 1995; Sprovieri et al., 2003; Rohling et al., 2004; Di Donato et al., 2019). Cool conditions have also been observed in the geochemical records from the North Ionian Sea (Filippidi and De Lange, 2019) and from the South Adriatic Sea (Siani et al., 2013) during the same interval. This phenomenon has been related to a long-term period of severe winter outbreaks of cold and dry northeast winds (Rohling et al., 2002), which drove the resumption of ADW formation (Piva et al., 2008; Marino et al., 2009; Siani et al., 2013; Filippidi and De Lange, 2019). Noteworthy is the strengthened contribution of Eastern Mediterranean deep waters recorded in the NDT-6-2016 core (Western Sicily Channel) (Fig. 1a) between 7 and 6 ky BP. This has been attributed to convection processes in the deep water formation cells of the Adriatic and Aegean Seas following the termination of the stagnant conditions that characterised S1 formation in the Central and Eastern Mediterranean (Trias-Navarro et al., 2023).

After the end of S1c, the abrupt shift of the K/Al curve towards higher values (Fig. 7) may be due to a Po riverine system's more prominent signature at the study site. This signal emerged following the maximum marine transgression after c.a. 7 ky BP and gradually decreased as a response to sea level stabilisation and concurrent reduction of glacier retreat episodes in Central Alps (e.g. Rossi and Vaiani, 2008; Siani et al., 2013; Amorosi et al., 2019). This general framework is also sustained by the $\delta^{13}C_{G.\ ruber\ white}$ that shows a sharp value drop recorded during the same short interval (6.6–6.3 ky BP) indicating the release of nutrient-rich waters, likely associated with enhanced riverine runoff (e.g. Mackensen and Schmiedl, 2019 and references therein) (Fig. 8). The calcareous nannofossil taxon *S. pulchra* responded promptly to the release of higher nutrient concentrations (Ziveri and Thunell, 2000; Ziveri et al., 2004; Triantaphyllou et al., 2004; Crudeli et al., 2023; Bonomo et al., 2017), despite the transition towards a cooler climate. However, its values along those of *B. bigelowii* decrease towards the end of cluster C (Fig. 8), mirroring the reducing trends of freshwater proxies (Ca/Ti, reworked) and suggesting the transition towards drier-cooler climate and/or hydrological modifications (e.g. Piva et al., 2008; Magny et al., 2013). This general framework could have been influenced by the southward migration of the Inter Tropical Convergence Zone (ITCZ), which drove drier climatic conditions over the Mediterranean basin in accordance with the progressive onset of the Bond event 4 and the corresponding development of a slightly negative NAO index (e.g. Lechleitner et al., 2017). In contrast, the Eastern Mediterranean experienced wetter conditions since c.a. 6 ky BP, which were linked to the formation of the mid-Holocene Sapropel layer (Triantaphyllou et al., 2014). A climatic seesaw between the Western and Eastern Mediterranean basins has been proposed as the main mechanism, likely driven by a reorganisation of large-scale atmospheric circulation (Roberts et al., 2011). In particular, the southward migration of the ITCZ in the tropics could have reinforced the mid-Holocene South Asian monsoon activity, albeit weak (Thamban et al., 2007), leading to the development of wetter conditions in the Aegean Sea (Triantaphyllou et al., 2014).

5.2. The 4.2 ky BP event

Between 5.4 and 4.1 ky BP, the general characteristics of calcareous nannofossil assemblages underwent changes following the onset of Cluster D (Fig. 7). This interval is defined by the development of dry conditions, as evidenced by the XRF (Ca/Ti, K/Al) and reworked coccolith decreased curves, which indicate reduced continental material deposition (e.g. Negri et al., 1999; Bonomo et al., 2016) and, consequently, lower nutrient inputs (i.e. higher $\delta^{13}C_{G.\ ruber\ white}$ values) (Fig. 7). In the Mediterranean basin, the development of widespread arid conditions has been generally observed in marine and continental records soon after the end of the African Humid Period (e.g., Rohling et al., 2002; Peyron et al., 2011, 2017; Siani et al., 2013; Goudeau et al., 2015). In the study record, between 4.7 and 4.3 ky BP, the sharp increase in the calcareous nannofossil cold water group abundance, associated with reduced continental input, points to the onset of cooler and drier conditions (Bond Event 3) (Fig. 7). On the other hand, the $\delta^{18}O_{G.\ ruber\ white}$ signal suggests the development of slightly warmer and wetter conditions (Fig. 7). This evidence suggests that the isotopic signal of *G. ruber* at the site could reflect a simultaneous dependence on seasonally driven conditions, likely recording summer and/or autumn information (e.g. Pujol and Vergnaud Grazzini, 1995; Rigual-Hernández et al., 2012; Mallo et al., 2017).

These climatic features chronologically coincide with the so-called "4.2 ky event", consistent with the timeframe reported by Bini et al. (2019) and described on average as an interval characterised by generally dry and cool conditions in the Central Mediterranean Basin. In addition, the development of a harsher climate determined a significant decline in the calcareous nannofossil warm water group, holococcoliths, and *S. pulchra* (Fig. 7), pointing to the development of cool and mixed water conditions (e.g., Ziveri et al., 2004; Margaritelli et al., 2020; Incarbona et al., 2023). Margaritelli et al. (2022) suggested that the formation of a winter mixed layer in the Western Mediterranean was connected to an atmospheric blocking event during the 4.2 ky event (Persoiu et al., 2019), driven by a strengthened Siberian High, which likely influenced the structure of the water column further east, including the planktonic foraminiferal assemblage composition. The comparison of our dataset with the reconstructed NAO index (Smith et al., 2016) shows that the identified 4.2 ky episode coincided with a positive NAO phase (Fig. 7), corresponding to the "4.2 ky drought" described for the Western Mediterranean (Cullen et al., 2000; Morellon et al., 2009). In the Aegean Sea, the 4.2 ky cold and dry event also marked the end of the warm and wet conditions interval that persisted since c.a. 6 ky BP, defining the onset of more arid conditions in the Eastern Mediterranean (Triantaphyllou et al., 2014).

Our findings are in accordance with records from both marine (e.g., Giunta et al., 2001; Emeis et al., 2003; Essallami et al., 2007; Margaritelli et al., 2016) and continental archives in the Central Mediterranean (e.g., Leng et al., 2001; Di Rita and Magri, 2009; Peyron et al., 2011, 2017; Zanchetta et al., 2012), confirming the regional climatic impact of this cool event. The end of the 4.2 ky climate event, at our study site, marks a major reorganisation in calcareous nannofossil assemblage as highlighted by the principal break in the dendrogram of the cluster analysis (boundary between cluster D and E) (Fig. 7), due to the sharp decline in the abundance of calcareous nannofossil cool species. At the same time, the amplification of the holococcoliths and K/Al signals is remarkable and, to some extent, appears to be associated with the intensification of NAO index, particularly in concomitance with negative oscillations (Fig. 7). In general, this framework aligns well with the broader transition of a significant shift in the Holocene climate, characterised by the amplification of millennial-scale oscillations (Bini et al., 2019; Català et al., 2019 and references therein).

5.3. Pre-Roman Period (4.1–2 ky BP)

As suggested by Margaritelli et al. (2020), the Pre-Roman Period, and particularly the time interval from ca. 4 ky BP to ca. 2 ky BP, is characterised by a long-term warming trend punctuated by an alternation of warmest events and short-term cooling ones. In the study record, the transition between clusters D and E is characterised by the development of warmer and slightly wetter climatic conditions as evidenced by an increase in calcareous nannofossil warm water group and holococcoliths abundances, and by relatively higher continental runoff, inferred from elevated Ca/Ti and K/Al ratios. Comparable conditions were also recorded in the calcareous nannofossil dataset in the Northwestern Mediterranean (Incarbona et al., 2023). This warm episode can be chronologically compared with the warm Early Bronze Age (EBA) climate event described in the Sicily Channel through Sea Surface Temperature (SST) Mg/Ca$_{G.\ ruber}$ reconstruction (Margaritelli et al., 2020).

Upwards (lower part of cluster E, 3.9–2.9 ky BP), low reworked values, decreasing trends in K/Al and Ca/Ti trends and sudden increase of $\delta^{13}C_{G.\ ruber\ \mathrm{white}}$ signal (Fig. 7) suggests the development of a short interval characterised by reduced runoff inputs, highlighting arid climate conditions, probably related to low Po riverine influence at the studied site. Similarly, in the Gulf of Taranto (North Ionian Sea), high $\delta^{13}C_{G.\ ruber\ \mathrm{white}}$ values were associated with a lower occurrence of the WAC as a consequence of a weakened Po riverine influence during the same interval (Goudeau et al., 2015). Finally, arid conditions were also documented in pollen records changes of the Southern Mediterranean area (Di Rita et al., 2018). Reduced riverine runoff could have affected the calcareous nannofossil *S. pulchra* (e.g. Ziveri et al., 2004; Malinverno et al., 2009; Skampa et al., 2020) which shows very low values throughout the middle part of the Bronze Age (Fig. 7). This arid climate condition occurs during cool climate as documented by the low abundance of calcareous nannofossil warm water group and holococcoliths (Fig. 7) and persisted throughout the middle part of the Bronze Age period (3.9–2.9 ky BP) as also documented in the Sicily Channel (Margaritelli et al., 2020).

Between 2.7 and 2.2 ky BP, the resolution of the study record is not able to document all the short-term climate changes documented by Margaritelli et al. (2020) but the recovery of calcareous nannofossil warm water group and holococcoliths, associated with light $\delta^{18}O_{G.\ ruber\ \mathrm{white}}$ values (Fig. 7) evidence the development of the prolonged warm phase from the Late Bronze Age to the Iron Age.

The decrease in abundance of calcareous nannofossil warm group between 2.2 and 2 ky BP allowed us to highlight cool climate conditions that chronologically correspond to the "sub-Atlantic" phase, which is characterised by cool and rainy winters (Kotthoff et al., 2017; Margaritelli et al., 2020). The impact of wetter winters during this period could be documented by increased holococcoliths values likely due to their enhanced preservation within sediments (e.g. Incarbona et al., 2023) and by the $\delta^{13}C_{G.\ ruber\ \mathrm{white}}$ ratio transition towards lower values, likely linked to the release of nutrient-rich continental runoff (e.g. Mackensen and Schmiedl, 2019). As a consequence, *S. pulchra* responded to the higher nutrient input with increased trend (e.g. Skampa et al., 2020; Crudeli et al., 2023) (Fig. 7). Similar features were observed in planktonic foraminiferal assemblages of the Tyrrhenian basin, where it was evidenced a shift towards higher productivity surface waters, stronger seasonality, and the increase of continental runoff (Lirer et al., 2014; Margaritelli et al., 2016). At our study site, the increasing K/Al and Ca/Ti trends suggest enhanced riverine runoff conditions concomitantly with the development of a prominent negative NAO phase (Fig. 7). However, the reworked curve does not sustain this evidence as it further decreases during this time interval. Between 4 and 2 ky BP, the transition of the Po River delta from a wave-dominated to a river-dominated coastal system was described (Amorosi et al., 2019). In this scenario, the shifting from coarse-grained to fine-grained sediment accumulation in the Po Delta could have trapped a portion of the finer sediment which did not reach our study site.

5.4. Roman Period (2–1.5 ky BP)

The Roman Period was generally described as a warm climatic phase (Margaritelli et al., 2020, and reference therein) during which we recorded an increase in the calcareous nannofossil warm water group and the shift towards lighter values of the $\delta^{18}O_{G.\ ruber\ \mathrm{white}}$ signal (Fig. 7). In addition, during this period, reduced riverine runoff is documented by relatively low reworked abundance and reduced K/Al and Ca/Ti trends (Fig. 7). The development of warmer conditions has been also observed in the coccolithophore assemblages of the Southern Adriatic Basin (Cascella et al., 2019). The peaks of *S. pulchra* at c.a. 2.1 and 1.6 ky BP could be evidence of punctual wetter intervals (e.g. Bonomo et al., 2017), coinciding with the wet-dry-wet seesaw events of the Dermody et al. (2012) models produced for the Central Mediterranean. Furthermore, the positive NAO index during this phase (Fig. 7) supports this general framework, which is characterised by persistent aridity in the Central Mediterranean (e.g. Magny et al., 2013), North Africa and Southern Europe (e.g. Margaritelli et al., 2020).

5.5. Post-Roman Period: (1.5–0 ky BP)

The Post-Roman Period is generally characterised by a progressive cooling trend, ending with the Little Ice Age (Margaritelli et al., 2018, 2020; Lirer et al., 2019), and interbedded by short-term climate events. In the study record, the general cooling is documented by the progressive shift of $\delta^{18}O_{G.\ ruber\ \mathrm{white}}$ towards heavier values, the slightly increase in calcareous nannofossil cold water group and lower values of the calcareous nannofossil warm water group (mainly between 1.5 and 0.5 ky BP) (Fig. 7). At the end of the Roman Period, the sharp decrease in the calcareous nannofossil warm water group and the progressive shift of $\delta^{18}O_{G.\ ruber\ \mathrm{white}}$ signal towards heavier values (Fig. 7) mark the onset of a short-time cooling event (1.5–1.35 ky BP) that chronologically corresponds to the Late Antique Little Ice Age (LALIA) event as documented in the Sicily Channel by Margaritelli et al. (2020).

Upwards, following the general cooling trend from the end of the LALIA (1.35 ky BP) to the top of the core, a progressive increase in reworked coccoliths is observed, accompanied by rising K/Al values (Fig. 7). This pattern may reflect enhanced continental discharge of detrital material from the Alps and Northern Apennines (e.g., Magny et al., 2013) under a negative NAO phase (Smith et al., 2016) (Fig. 7), suggesting the establishment of wetter climatic conditions. Concomitantly, higher values of the Ca/Ti ratio can suggest higher release of carbonate debris at the study site, resulting from the higher subaerial erosion of the Apulian margin likely linked to anthropogenic deforestation (e.g. Kaplan et al., 2009). In this context, higher holococcolith values (Fig. 7) may indicate deep water production. In the Western Mediterranean, increased holococcolith abundance has been observed during the negative NAO phases recorded by the Cueva de Asiul speleothem (Incarbona et al., 2023). These authors suggested that increased North Spain rainfall could have been driven by strengthened and prolonged westerlies, possibly due to persistent blocking events impacting Western Europe, triggering deep water formation and seafloor ventilation (Incarbona et al., 2023 and references therein). We suggest that a similar mechanism may have influenced our study area, promoting seafloor ventilation and holococcolith preservation during this interval. Soon after, the shift of $\delta^{18}O_{G.\ ruber\ \mathrm{white}}$ signal towards lighter values (Fig. 7) seems to suggest the occurrence of a warm/wet event (1.35–0.6 ky BP) that we could speculate chronologically corresponds to the Medieval Climate Anomaly (MCA) period (Fig. 7).

In the study record, the decrease in abundance of calcareous nannofossil warm water taxa and the increase of the cold water ones, defines the development of a generally cooler climate (Fig. 7). Similar paleoenvironmental and palaeoceanographic features were deduced in the last part of the MCA from the study of the calcareous nannofossils of the Balearic Sea (1–0.7 ky BP) (Incarbona et al., 2023), planktonic foraminiferal assemblages of the Tyrrhenian Basin during winter months (Margaritelli et al., 2016) and of the Menorca Basin during the short-term Medieval Cool Event (Margaritelli et al., 2018). In the Central Mediterranean, the MCA has been described as formed by two distinct phases (Goudeau et al., 2015), where cooler conditions characterised the initial part (Medieval Cold Event), while a warmer climate was recorded during the second phase (Medieval Warm Event) (Lirer et al., 2014, 2019; Margaritelli et al., 2016, 2018; Mensing et al., 2016; Cascella et al., 2019). Nevertheless, the Medieval cooler phase exhibited a more pronounced signature (Margaritelli et al., 2016, 2018; Lirer et al., 2019; Lüning et al., 2019). It is thus plausible that at our study site, the warmer coccolithophorid assemblages did not fully recover from the LALIA cool interval, continuing to exhibit lower values throughout the MCA interval (Fig. 7). The cool conditions highlighted by the $\delta^{18}O_{G.\ ruber\ \mathrm{white}}$ heavy values, persisted up to c.a. 0.3 ky BP (Fig. 7). In particular, the drop of holococcoliths abundance and the slight increase of the cold water group are coeval to the Little Ice Age (LIA) event described by Margaritelli et al. (2020) and concomitant with the onset of the Bond event 0 (Fig. 7). However, despite the development of cooler climatic conditions, the warm water group values increased (Fig. 7), likely attesting the transition of the trophic features of the water column from higher to lower coccolithophorid productivity conditions (e.g. Triantaphyllou et al., 2004; Dimiza et al., 2008; Oviedo et al., 2015; Bonomo et al., 2021). A similar response of the coccolithophorid community was recorded in the Southern Adriatic Sea (Cascella et al., 2019) and in the North Aegean Sea (Gogou et al., 2016; Skampa et al., 2019) where the foraminifera benthic community also recorded a shift towards oligo-mesotrophic conditions (see Dimiza et al., 2020). Also in the Tyrrhenian Sea, a transition in nutrient availability in the water column is marked by the shift from carnivorous to herbivorous-opportunistic planktonic foraminifera taxa (Lirer et al., 2014; Margaritelli et al., 2016). The gradual increasing trend in K/Al ratio and of reworked abundance, indicate enhanced riverine runoff which sustained the relatively high values of *S. pulchra* taxon (e.g. Flores et al., 1997; Colmenero-Hidalgo et al., 2004; Dimiza et al., 2008, 2015; Malinverno et al., 2009, 2014) (Fig. 7). At the same time, slightly decreasing trend of $\delta^{13}C_{G.\ ruber\ \mathrm{white}}$ values suggest the release of nutrient-rich waters likely due to the strengthened WAC outflow over the year (Goudeau et al., 2015) during a supposed wetter late LIA (e.g. Grove, 2001; Nicault et al., 2008; Grauel et al., 2013). Nevertheless, the persistent positive NAO phase reconstructed by Smith et al. (2016) (Fig. 7) does not match with the proxies of enhanced continental runoff recorded during this interval (Bonomo et al., 2016; Cascella et al., 2019). Within this framework, anthropogenic pressure during the LIA could have driven higher fluvial discharge (e.g., Piccarreta et al., 2011; Wirth et al., 2013; Benito et al., 2015). However, NAO reconstructions may be influenced by several factors, such as the proxies used, local precipitation patterns, and applied models, among others, which could result in discrepancies when comparing some events. For instance, during the same interval, negative NAO phases have been described by Trouet et al. (2009), Olsen et al. (2012), and Faust et al. (2016). Nonetheless, the findings from our study are consistent with those of Incarbona et al. (2023) in the Balearic Sea, showing enhanced holococcolith preservation during the negative NAO phases reconstructed by Smith et al. (2016), and vice versa still suggesting a common response between North Iberian and Western-Central Mediterranean climatic settings (Fig. 7). After the LIA, the shift in $\delta^{18}O_{G.\ ruber\ \mathrm{white}}$ signal towards less positive values evidence a sharp transition towards warmer climate conditions (Fig. 7) as suggested by Lirer et al. (2019) and Margaritelli et al. (2018). However, the trend reverses near at top of the record, pointing to a return to harsher climatic conditions and/or the onset of a drier climate. Indeed, the reduced influence of riverine runoff is supported by the lower values of reworked material and the K/Al ratio (Fig. 7). Additionally, the shift of $\delta^{13}C_{G.\ ruber\ \mathrm{white}}$ towards more positive values indicates a decline in nutrient-rich water input, which is reflected in the negative response of *S. pulchra* (Fig. 7).

6. Conclusions

The multiproxy study of the ND14Mbis gravity core based on micropaleontological, geochemical and XRF data provided valuable information on the climatic events developed in the North Ionian Basin during the past 10 ky, where the general climatic configuration appeared to be influenced by both North Atlantic and African climatic systems. In particular, the 1.6 ky periodicity extrapolated from the cold water group IMF3 signal suggested the influence of the North Atlantic 1.5 ky Bond cycles at the study site.

The oscillations of the calcareous nannofossil assemblage, combined with cluster analysis, identified key paleontological and paleoenvironmental changes at the study site. In particular, this approach allowed us to state that Sapropel 1 deposition at the study site lasted until 6.6 ky BP, despite the lack of sedimentary evidence (e.g. oxidised sediments). During the S1 event, the dysoxic bottom-water conditions (e.g. Giunta et al., 2003; Filippidi and De Lange, 2019) were interrupted during two short spells of climate cooling that chronologically correspond with the well-known 8.2 and 7.4 ky BP events. After the 7.4 ky BP event, indications of weak stratified conditions in the water column developed, as highlighted by the relatively higher values of the taxa of *F. profunda*, *S. pulchra* and *B. bigelowii*. After the end of S1 (6.6 ky BP), prominent mixing conditions were marked by the sharp shift of the $\delta^{18}O_{G.\ ruber\ \mathrm{white}}$ towards heavier values evidencing the resumption of Adriatic Deep Water formation. Concomitantly, a lower $\delta^{13}C_{G.\ ruber\ \mathrm{white}}$ ratio and higher K/Al values pointed to a stronger Po riverine imprint. Under these conditions, *G. scitula* and *N. incompta* planktonic foraminifera, indicative of cool and well-mixed waters, showed increased trends. Subsequent freshwater input (reworked coccoliths, *S. pulchra*, K/Al) and nutrient concentrations ($\delta^{13}C_{G.\ ruber\ \mathrm{white}}$) proxy variations evidenced the transition towards drier conditions, marking the end of the African Humid Period at our study site (10–5.4 ky BP).

At the 4.2 ky BP threshold, the cluster analysis outcomes, along with the calcareous nannofossil configuration, suggest a major reorganisation of the climatic system at our study site, likely modulated by a stronger influence of the NAO. This transition marked the shift towards stronger NAO phases, as recorded in Northern Iberia (Smith et al., 2016). Comparisons with the calcareous nannofossil assemblage and the XRF dataset revealed that NAO oscillations directly affected the holococcolith abundance and K/Al trends, with higher values associated with negative NAO phases.

From 4.2 ky BP onwards, calcareous nannofossil distribution registered shorter-lived climatic events within the Pre-Roman (4.1–2 ky BP), Roman (2–1.5 ky BP) and Post-Roman (1.5–0 ky BP) Periods. Particularly, the coccolithophorid assemblage registered the cooler climatic events more prominently than other proxies at our study site, i.e. emphasising the cooler portion of the Medieval Climate Anomaly. Finally, during the Little Ice Age (0.5–0.3 ky BP), increased abundances of the warm water group suggested a shift towards lower coccolithophorid productivity, likely associated with enhanced riverine runoff as indicated by reworked coccoliths and XRF elemental data. These conditions led to the onset of density-stratified waters, a phenomenon also recorded by the coccolithophore assemblages in the Adriatic Basin (Cascella et al., 2019) and in the North Aegean Sea (Gogou et al., 2016; Skampa et al., 2019) during the same interval.

CRediT authorship contribution statement

L. Bronzo: Writing – review & editing, Writing – original draft, Investigation, Formal analysis, Conceptualization. **A. Cascella:** Writing – review & editing, Supervision, Funding acquisition, Conceptualization. **S. Bonomo:** Writing – review & editing, Formal analysis. **C. Morigi:** Writing – review & editing, Supervision. **I. Cacho:** Writing – review & editing, Funding acquisition. **G. Margaritelli:** Writing – review & editing. **J. Frigola:** Writing – review & editing. **L.D. Pena:** Writing – review & editing. **F. Lirer:** Writing – review & editing, Supervision, Project administration, Funding acquisition.

Declaration of competing interest

The authors declare that they have no known competing financial interests or personal relationships that could have appeared to influence the work reported in this paper.

Acknowledgements

We acknowledge the financial support provided by the ERC-Consolidator TIMED project (REP-683237), the INGV project 2019 (Paleoclimate variability during Late Holocene in the Central Mediterranean and Balkans: terrestrial and marine archive comparison) and the Pegaso PhD grant 2021 provided by Tuscany Region (Italy) through Università degli Studi di Firenze. The marine core ND14Mbis has been collected by ISMAR-CNR (Napoli) aboard of the R/V CNR-Urania. This research has been financially supported by the Project of Strategic Interest NextData PNR2011–2013 (http://www.nextdataproject.it). We acknowledge Prof. Antonio Caruso and the two anonymous reviewers for their valuable suggestions that improved the quality of the work.

Appendix A. Supplementary data

Supplementary data to this article can be found online at https://doi.org/10.1016/j.palaeo.2025.112977.

Data availability

Data will be made available on request.

References

Amore, O.F., Caffau, M., Massa, B., Morabito, S., 2004. Late pleistocene–holocene paleoclimate and related paleoenvironmental changes as recorded by calcareous nannofossils and planktonic foraminifera assemblages in the Southern Tyrrhenian Sea (Cape Palinuro, Italy). Mar. Micropaleontol. 52 (1–4), 255–276. https://doi.org/10.1016/J.MARMICRO.2004.05.004.

Amorosi, A., Barbieri, G., Bruno, L., Campo, B., Drexler, T.M., Hong, W., Rossi, V., Sammartino, I., Scarponi, D., Vaiani, S.C., Bohacs, K.M., 2019. Three-fold nature of coastal progradation during the Holocene eustatic highstand, Po Plain, Italy–close correspondence of stratal character with distribution patterns. Sedimentology 66 (7), 3029–3052.

Argenio, C., Flores, J.-A., Balestra, B., Cerulo, L., Cachão, M., Amore, F.O., 2024. Surface water mass dynamics at IODP site U1313 through principal component analysis: evidence from coccolith assemblages in the ~25–7 Kyr interval. Palaeogeogr. Palaeoclimatol. Palaeoecol. 635, 111960. https://doi.org/10.1016/J.PALAEO.2023.111960.

Athanasiou, M., Bouloubassi, I., Gogou, A., Klein, V., Dimiza, M.D., Parinos, C., Skampa, E., Triantaphyllou, M.V., 2017. Sea surface temperatures and environmental conditions during the "warm Pliocene" interval (~ 4.1–3.2 Ma) in the Eastern Mediterranean (Cyprus). Glob. Planet. Chang. 150, 46–57. https://doi.org/10.1016/J.GLOPLACHA.2017.01.008.

Ausín, B., Flores, J.-A., Sierro, F.J., Cacho, I., Hernández-Almeida, I., Martrat, B., Grimalt, J.O., 2015. Atmospheric patterns driving holocene productivity in the Alboran Sea (Western Mediterranean): a multiproxy approach. Holocene 25 (4), 583–595. https://doi.org/10.1177/0959683614565952.

Bazzicalupo, P., Sicre, M.A., Checa, H., Maiorano, P., Margaritelli, G., Klein, V., Pena, L. D., Cacho, I., Frigola, J., Bonomo, S., Cascella, A., Lirer, F., 2022. Climate evolution in the Adriatic Sea across the last deglaciation: a multiproxy approach combining biomarkers and calcareous plankton. Palaeogeogr. Palaeoclimatol. Palaeoecol. 608. https://doi.org/10.1016/j.palaeo.2022.111291.

Benito, G., Macklin, M.G., Zielhofer, C., Jones, A.F., Machado, M.J., 2015. Holocene flooding and climate change in the Mediterranean. Catena 130, 13–33. https://doi.org/10.1016/j.catena.2014.11.014.

Bignami, F., Sciarra, R., Carniel, S., Santoleri, R., 2007. Variability of Adriatic Sea coastal turbid waters from SeaWiFS imagery. J. Geophys. Res. Oceans 112 (C3). https://doi.org/10.1029/2006JC003518.

Bini, M., Zanchetta, G., Perşoiu, A., Cartier, R., Català, A., Cacho, I., Dean, J.R., Di Rita, F., Drysdale, R., Finnè, M., Isola, I., Jalali, B., Lirer, F., Magri, D., Masi, A., Marks, L., Mercuri, A., Peyron, O., Sadori, L., Sicre, M., Welc, F., Zielhofer, C., Brisset, E., 2019. The 4.2 Ka BP event in the Mediterranean region: an overview. Clim. Past 15 (2), 555–577. https://doi.org/10.5194/cp-15-555-2019.

Bolle, H.-J., 2003. Climate, climate variability, and impacts in the Mediterranean area: an overview. Mediter. Clim. 5–86. https://doi.org/10.1007/978-3-642-55657-9_2.

Bond, G., Kromer, B., Beer, J., Muscheler, R., Evans, M.N., Showers, W., Hoffmann, S., Lotti-Bond, R., Hajdas, I., Bonani, G., 2001. Persistent solar influence on North Atlantic climate during the holocene. Science 294 (5549), 2130–2136. https://doi.org/10.1126/science.1065680.

Bonomo, S., Cascella, A., Alberico, I., Ferraro, L., Giordano, L., Lirer, F., Vallefuoco, M., Marsella, E., 2014. Coccolithophores from near the volturno estuary (Central Tyrrhenian Sea). Mar. Micropaleontol. 111, 26–37. https://doi.org/10.1016/j.marmicro.2014.06.001.

Bonomo, S., Cascella, A., Alberico, I., Sorgato, S., Pelosi, N., Ferraro, L., Lirer, F., Vallefuoco, M., Bellucci, L., Agnini, C., Pappone, G., 2016. Reworked coccoliths as runoff proxy for the last 400 years: the case of Gaeta Gulf (Central Tyrrhenian Sea, Central Italy). Palaeogeogr. Palaeoclimatol. Palaeoecol. 459, 15–28. https://doi.org/10.1016/J.PALAEO.2016.06.037.

Bonomo, S., Placenti, F., Quinci, E.M., Cuttitta, A., Genovese, S., Mazzola, S., Bonanno, A., 2017. Living coccolithophores community from southern Tyrrhenian Sea (Central Mediterranean — Summer 2009). Mar. Micropaleontol. 131, 10–24. https://doi.org/10.1016/J.MARMICRO.2017.02.002.

Bonomo, S., Schroeder, K., Cascella, A., Alberico, I., Lirer, F., 2021. Living coccolithophore communities in the central Mediterranean Sea (Summer 2016): relations between ecology and oceanography. Mar. Micropaleontol. 165. https://doi.org/10.1016/j.marmicro.2021.101995.

Borzelli, G., Eusebi, L., Gačič, M., Cardin, V., Civitarese, G., 2009. Eastern Mediterranean transient and reversal of the Ionian Sea circulation. Geophys. Res. Lett. 36 (15), 15108. https://doi.org/10.1029/2009GL039261.

Bown, P.R. (Ed.), 1998. Calcareous Nannofossil Biostratigraphy. Chapman & Hall, London. https://link.springer.com/book/9780412789700.

Broecker, W.S., 2001. Paleoclimate: was the medieval warm period global? Science 291 (5508), 1497–1499. https://doi.org/10.1126/SCIENCE.291.5508.1497.

Bukry, D., 1973. Phytoplankton stratigraphy, deep sea drilling project leg 20, Western Pacific Ocean. In: Hezeen, B.C., McGregor, I.D. (Eds.), Initial Reports of the Deep Sea Drilling Project. Government Printing Office, U.S, pp. 307–317.

Bunn, A.G., 2010. Statistical and visual crossdating in R using the DplR Library. Dendrochronologia 28 (4), 251–258.

Burrough, S.L., D. S., Thomas., 2013. Central Southern Africa at the time of the African Humid Period: a new analysis of Holocene palaeoenvironmental and palaeoclimate data. Quat. Sci. Rev. 80, 29–46.

Calvert, S.E., Pedersen, T.F., 2007. Chapter fourteen elemental proxies for palaeoclimatic and palaeoceanographic variability in marine sediments: interpretation and application. Dev. Marine Geol. 1, 567–644. https://doi.org/10.1016/S15725480(07)01019-6.

Cascella, A., Bonomo, S., Jalali, B., Sicre, M.A., Pelosi, N., Schmidt, S., Lirer, F., 2019. Climate variability of the last ~2700 years in the Southern Adriatic Sea: coccolithophore evidences. Holocene 30 (1), 53–64. https://doi.org/10.1177/0959683619865600.

Cascella, A., Bonomo, S., Lirer, F., Margaritelli, G., Checa, H., Cacho, I., Pena, L.D., Frigola, J., 2021. The response of calcareous plankton to the Sapropel S1 interval in North Ionian Sea. Glob. Planet. Chang. 205. https://doi.org/10.1016/j.gloplacha.2021.103599.

Casford, J.S.L., Rohling, E.J., Abu-Zied, R., Cooke, S., Fontanier, C., Leng, M., Lykousis, V., 2002. Circulation changes and nutrient concentrations in the late Quaternary Aegean Sea: a nonsteady state concept for sapropel formation. Paleoceanography 17 (2), 14–21.

Casford, J.S.L., Rohling, E.J., Abu-Zied, R.H., Fontanier, C., Jorissen, F.J., Leng, M.J., Schmiedl, G., J., Thomson., 2003. A dynamic concept for eastern Mediterranean circulation and oxygenation during sapropel formation. Palaeogeogr. Palaeoclimatol. Palaeoecol. 190, 103–119.

Català, A., Cacho, I., Frigola, J., Pena, L.D., Lirer, F., 2019. Holocene hydrography evolution in the Alboran Sea: a multi-record and multi-proxy comparison. Clim. Past 15, 927–942. https://doi.org/10.5194/cp-15-927-2019.

Checa, H., Margaritelli, G., Pena, L.D., Frigola, J., Cacho, I., Rettori, R., Lirer, F., 2020. High resolution paleo-environmental changes during the sapropel 1 in the North Ionian Sea, Central Mediterranean. Holocene 30 (11), 1504–1515. https://doi.org/10.1177/0959683620941095.

Cheshire, H., Jü, J., Thurow, J., Nederbragt, A.J., Cheshire, H., Nederbragt, J., 2005. Late quaternary climate change record from two long sediment cores from Guaymas Basin, Gulf of California. J. Quat. Sci. 20 (5), 457–469. https://doi.org/10.1002/JQS.944.

Cisneros, M., Cacho, I., Frigola, J., Canals, M., Masqué, P., Martrat, B., Casado, M., Grimalt, J.O., Pena, L.D., Margaritelli, G., Lirer, F., 2016. Sea surface temperature variability in the central-western Mediterranean Sea during the last 2700 years: a multi-proxy and multi-record approach. Clim. Past 12 (4), 849–869. https://doi.org/10.5194/CP-12-849-2016.

Civitarese, G., Gačić, M., Lipizer, M., Eusebi Borzelli, G.L., 2010. On the impact of the bimodal oscillating system (BiOS) on the biogeochemistry and biology of the Adriatic and Ionian Seas (Eastern Mediterranean). Biogeosciences 7 (12), 3987–3997. https://doi.org/10.5194/bg-7-3987-2010.

Colmenero-Hidalgo, E., Flores, J.-A., Sierro, F.J., 2002. Biometry of *Emiliania huxleyi* and its biostratigraphic significance in the eastern north Atlantic Ocean and Western Mediterranean Sea in the last 20 000 years. Mar. Micropaleontol. 46 (3–4), 247–263. https://doi.org/10.1016/S0377-8398(02)00065-8.

Colmenero-Hidalgo, E., Flores, J.-A., Sierro, F.J., Bárcena, M.Á., Löwemark, L., Schönfeld, J., Grimalt, J.O., 2004. Ocean surface water response to short-term climate changes revealed by coccolithophores from the Gulf of Cadiz (NE Atlantic) and Alboran Sea (W Mediterranean). Palaeogeogr. Palaeoclimatol. Palaeoecol. 205 (3–4), 317–336. https://doi.org/10.1016/J.PALAEO.2003.12.014.

Crow, E.L., Davis, F.A., Maxfield, M.W., 1960. Statistics Manual. Inc. Dover Publications, New York.

Crudeli, D., Young, J.R., Erba, E., Geisen, M., Ziveri, P., De Lange, G.J., Slomp, C.P., 2023. Fossil Record of Holococcoliths and Selected Hetero-Holococcolith Associations from the Mediterranean (Holocene-Late Pleistocene): Evaluation of Carbonate Diagenesis and Palaeoecological-Palaeocenographic Implications. https://doi.org/10.1016/j.palaeo.2005.11.022.

Cullen, H.M., de Menocal, P.B., Hemming, S., Brown, F.H., Guilderson, T., Sirocko, F., 2000. Climate change and the collapse of the Akkadian empire: evidence from the deep sea. Geology 28 (4), 379–382. https://doi.org/10.1130/0091-7613(2000)28%3C379:CCATCO%3E2.0.CO;2.

D'Amario, B., Ziveri, P., Grelaud, M., Oviedo, A., Kralj, M., 2017. Coccolithophore haploid and diploid distribution patterns in the Mediterranean Sea: can a haplo-diploid life cycle be advantageous under climate change? J. Plankton Res. 39 (5), 781–794. https://doi.org/10.1093/PLANKT/FBX044.

De Beaulieu, J.L., Miras, Y., Andrieu-Ponel, V., Guiter, F., 2005. Vegetation dynamics in North-Western Mediterranean regions: instability of the mediterranean bioclimate. Plant Biosyst. 139 (2), 114–126. https://doi.org/10.1080/11263500500197858.

De Lange, G.J., Thomson, J., Reitz, A., Slomp, C.P., Speranza Principato, M., Erba, E., Corselli, C., 2008. Synchronous basin-wide formation and redox-controlled preservation of a Mediterranean Sapropel. Nat. Geosci. 1 (9), 606–610. https://doi.org/10.1038/ngeo283.

Debret, M., Bout-Roumazeilles, V., Grousset, F., Desmet, M., McManus, J.F., Massei, N., Sebag, D., Petit, J.-R., Copard, Y., Trentesaux, A., 2007. Climate of the Past The Origin of the 1500-Year Climate Cycles in Holocene North-Atlantic Records, 3, pp. 569–575. www.clim-past.net/3/569/2007/.

Debret, M., Sebag, D., Crosta, X., Massei, N., Petit, J.R., Chapron, E., Bout-Roumazeilles, V., 2009. Evidence from wavelet analysis for a mid-holocene transition in global climate forcing. Quat. Sci. Rev. 28 (25–26), 2675–2688. https://doi.org/10.1016/j.quascirev.2009.06.005.

DeMenocal, P., Ortiz, J., Guilderson, T., Sarnthein, M., 2000. Coherent high- and low-latitude climate variability during the holocene warm period. Science 288 (5474), 2198–2202. https://doi.org/10.1126/SCIENCE.288.5474.2198.

Dermody, B.J., De Boer, H.J., Bierkens, M.F.P., Weber, S.L., Wassen, M.J., Dekker, S.C., 2012. A seesaw in Mediterranean precipitation during the Roman Period linked to millennial-scale changes in the North Atlantic. Clim. Past 8 (2), 637–651. https://doi.org/10.5194/CP-8-637-2012.

Desprat, S., Combourieu-Nebout, N., Essallami, L., Sicre, M.A., Dormoy, I., Peyron, O., Siani, G., Bout Roumazeilles, V., Turon, J.L., 2013. Deglacial and Holocene vegetation and climatic changes in the southern Central Mediterranean from a direct land–sea correlation. Clim. Past 9, 767–787. https://doi.org/10.5194/cp-9-767-2013.

Di Rita, F., Magri, D., 2009. Holocene drought, deforestation and evergreen vegetation development in the Central Mediterranean: a 5500 year record from Lago Alimini Piccolo, Apulia, Southeast Italy. Holocene 19 (2), 295–306. https://doi.org/10.1177/0959683608100574.

Di Donato, V., Insinga, D.D., Iorio, M., Molisso, F., Rumolo, P., Cardines, C., Passaro, S., 2019. The palaeoclimatic and palaeoceanographic history of the Gulf of Taranto (Mediterranean Sea) in the last 15 ky. Glo. Pla. Cha. 172, 278–297. https://doi.org/10.1016/j.gloplacha.2018.10.014.

Di Rita, F., Fletcher, W.J., Aranbarri, J., Margaritelli, G., Lirer, F., Magri, D., 2018. Holocene forest dynamics in central and western Mediterranean: periodicity, spatio-temporal patterns and climate influence. Sci. Rep. 8 (1), 1–13. https://doi.org/10.1038/s41598-018-27056-2.

Di Rita, F., Lirer, F., Margaritelli, G., Michelangeli, F., Magri, D., 2019. Climate and human influence on the vegetation of Tyrrhenian Italy during the last 2000 years: new insights from microcharcoal and non-pollen palynomorphs. Phys. Geogr. Quat. Dynamics 42 (2), 203–214. https://doi.org/10.4461/GFDQ.2019.42.10.

Di Stefano, E., Incarbona, A., 2004. High-resolution palaeoenvironmental reconstruction of ODP hole 963D (Sicily Channel) during the last deglaciation based on calcareous nannofossils. Mar. Micropaleontol. 52, 241–254. https://doi.org/10.1016/j.marmicro.2004.04.009.

Dimiza, M.D., Triantaphyllou, M., Dermitzakis, M.D., 2008. Seasonality and ecology of living coccolithophores in Eastern Mediterranean coastal environment (Andros Island, Middle Aegean Sea). Micropaleontology 54. https://www.jstor.org/stable/30130910.

Dimiza, M.D., Triantaphyllou, M.V., Malinverno, E., Psarra, S., Karatsolis, B.-T., Mara, P., Lagaria, A., Gogou, A., 2015. The composition and distribution of living coccolithophores in the Aegean Sea (NE Mediterranean). Extant Coccol. 61 (6). https://www.jstor.org/stable/44511374.

Dimiza, M.D., Fatourou, M., Arabas, A., Panagiotopoulos, I., Gogou, A., Kouli, K., Parinos, C., Rousakis, G., Triantaphyllou, M.V., 2020. Deep-sea benthic foraminifera record of the last 1500 years in the North Aegean Trough (northeastern Mediterranean): a paleoclimatic reconstruction scenario. Deep-Sea Res. II Top. Stud. Oceanogr. 171, 104705. https://doi.org/10.1016/J.DSR2.2019.104705.

Duplessy, J.C., Cortijo, E., Kallel, N., 2005. Marine records of Holocene climatic variations. Compt. Rendus Geosci. 337 (1–2), 87–95. https://doi.org/10.1016/j.crte.2004.08.007.

Emeis, K.C., Schulz, H., Struck, U., Rossignol-Strick, M., Erlenkeuser, H., Howell, M.W., Kroon, D., et al., 2003. Eastern Mediterranean surface water temperatures and $\delta^{18}O$ composition during deposition of sapropels in the late quaternary. Paleoceanography 18 (1). https://doi.org/10.1029/2000PA000617.

Essallami, L., Sicre, M.A., Kallel, N., Labeyrie, L., Siani, G., 2007. Hydrological changes in the Mediterranean Sea over the last 30,000 years. Geochem. Geophys. Geosyst. 8 (7). https://doi.org/10.1029/2007GC001587.

Faust, J.C., Fabian, K., Milzer, G., Giraudeau, J., Knies, J., 2016. Norwegian fjord sediments reveal NAO related winter temperature and precipitation changes of the past 2800 years. Earth Planet. Sci. Lett. 435 (1), 84–93. https://doi.org/10.1016/j.epsl.2015.12.003.

Ferraro, S., Sulli, A., Di Stefano, E., Giaramita, L., Incarbona, A., Mortyn, P.G., Sprovieri, M., Tonielli, R., Vallefuoco, M., Zizzo, E., Tranchida, G., 2018. Late quaternary palaeoenvironmental reconstruction of sediment drift accumulation in the Malta Graben (Central Mediterranean Sea). Geo-Mar. Lett. 38 (3), 241–258. https://doi.org/10.1007/S00367-018-0534-X.

Ferreira, J., Cachão, M., González, R., 2008. Reworked calcareous nannofossils as ocean dynamic tracers: the Guadiana Shelf Case Study (SW Iberia). Estuar. Coast. Shelf Sci. 79 (1), 59–70. https://doi.org/10.1016/J.ECSS.2008.03.012.

Filippidi, A., De Lange, G.J., 2019. Eastern mediterranean deep water formation during Sapropel S1: a reconstruction using geochemical records along a bathymetric transect in the adriatic outflow region. Paleoceanogr. Paleoclimatol. 34 (3), 409–429. https://doi.org/10.1029/2018PA003459.

Filippidi, A., Triantaphyllou, M.V., G. J., De Lange., 2016. Eastern-Mediterranean ventilation variability during sapropel S1 formation, evaluated at two sites influenced by deep-water formation from Adriatic and Aegean Seas. Quat. Sci. Rev. 144, 95–106.

Finkel, R.C., Nichiizumi, K., 1997. Beryllium 10 concentrations in the Greenland Ice Sheet Project 2 ice core from 3-40 ka. J. Geophys. Res. 2 (C12), 26699–26706.

Finné, M., Woodbridge, J., Labuhn, I., Roberts, C.N., 2019. Holocene hydro-climatic variability in the Mediterranean: a synthetic multi-proxy reconstruction. Holocene 29 (5), 847–863. https://doi.org/10.1177/0959683619826634.

Fletcher, W.J., Sanchez Goni, M.F., Peyron, O., Dormoy, I., 2010. Abrupt climate changes of the last deglaciation detected in a Western Mediterranean forest record. Clim. Past 6, 245–246.

Fletcher, W.J., Debret, M., Sanchez Goni, M.F., 2013. Mid-Holocene emergence of a low-frequency millennial oscillation in western Mediterranean climate: Implications for past dynamics of the North Atlantic atmospheric westerlies. Holocene 23 (2), 153–166. https://doi.org/10.1177/0959683612460783.

Flores, J.-A., Sierro, F.J., Francés, G., Vázquez, A., Zamarreno, I., 1997. The last 100,000 years in the Western Mediterranean: sea surface water and frontal dynamics as revealed by coccolithophores. Mar. Micropaleontol. 29 (3–4), 351–366. https://doi.org/10.1016/S0377-8398(96)00029-1.

Flores, J.-A., Gersonde, R., Sierro, F.J., 1999. Pleistocene fluctuations in the agulhas current retroflection based on the calcareous plankton record. Mar. Micropaleontol. 37 (1), 1–22. https://doi.org/10.1016/S0377-8398(99)00012-2.

Flores, J.-A., Colmenero-Hidalgo, E., Mejía-Molina, A.E., Baumann, K.-H., Henderiks, J., Larsson, K., Prabhu, C.N., Sierro, F.J., Rodrigues, T., 2010. Distribution of large *Emiliania huxleyi* in the Central and Northeast Atlantic as a tracer of surface ocean dynamics during the last 25,000years. Mar. Micropaleontol. 76 (3–4), 53–66. https://doi.org/10.1016/j.marmicro.2010.05.001.

Frigola, J., Moreno, A., Cacho, I., Miquel, Canals, Sierro, F.J., Flores, J.A., Grimalt, J.O., Hodell, D.A., Curtis, J.H., 2007. Holocene climate variability in the western Mediterranean region from a deepwater sediment record. Paleoceanography 22 (2). https://doi.org/10.1029/2006PA001307.

Frigola, J., Moreno, A., Cacho, I., Canals, M., Sierro, F.J., Flores, J.A., Grimalt, J.O., 2008. Evidence of abrupt changes in Western Mediterranean deep water circulation during the last 50 Kyr: a high-resolution marine record from the Balearic Sea. Quat. Int. 181 (1), 88–104. https://doi.org/10.1016/J.QUAINT.2007.06.016.

Gacic, M., Eusebi Borzelli, G.L., Civitarese, G., Cardin, V., Yari, S., 2010. Can internal processes sustain reversals of the ocean upper circulation? The Ionian Sea example. Geophys. Res. Lett. 37 (9). https://doi.org/10.1029/2010GL043216.

Gasse, F., 2000. Hydrological changes in the African Tropics since the last glacial maximum. Quat. Sci. Rev. 19 (1–5), 189–211. https://doi.org/10.1016/S0277-3791(99)00061-X.

Geraga, M., Tsaila-Monopolis, S., Papatheodorou, C.I.G., Ferentinos, G., 2005. Sorth-term climate changes in the southern Aegean Sea over the last 48,000 years. Palaeogeogr. Palaeoclimatol. Palaeoecol. 220, 311–332. https://doi.org/10.1016/J.PALAEO.2005.01.010.

Geraga, M., Mylona, G., Papatheodorou, G., G., Ferentinos., 2008. Northeastern Ionian Sea: palaeoceanographic variability over the last 22 ka. J. Mar. Syst. 74 (1–2), 623–638.

Giraudi, C., 2011. Chapter 17 – Middle pleistocene to holocene glaciations in the Italian apennines. In: Developments in Quaternary Sciences, 15, pp. 211–219. https://doi.org/10.1016/B978-0-444-53447-7.00017-9.

Giunta, S., Emeis, K.-C., Negri, A., 2001. Sea surface temperatures reconstruction of the last 16,000 years in the eastern Mediterranean Sea. Riv. Ital. Paleontol. Stratigr. 107 (3). https://doi.org/10.13130/2039-4942/5447.

Giunta, S., Negri, A., Morigi, C., Capotondi, L., Combourieu-Nebout, N., Emeis, K.C., Sangiorgi, F., Vigliotti, L., 2003. Coccolithophorid ecostratigraphy and multi-proxy paleoceanographic reconstruction in the Southern Adriatic Sea during the last deglacial time (Core AD91-17). Palaeogeogr. Palaeoclimatol. Palaeoecol. 190, 39–59. https://doi.org/10.1016/S0031-0182(02)00598-9.

Gogou, A., Bouloubassi, I., Lykousis, V., Arnaboldi, M., Gaitani, P., Meyers, P.A., 2007. Organic geochemical evidence of late Glacial-Holocene climate instability in the North Aegean Sea. Palaeogeogr. Palaeoclimatol. Palaeoecol. 256, 1–20. https://doi.org/10.1016/J.PALAEO.2007.08.002.

Gogou, A., Triantaphyllou, M., Xoplaki, E., Izdebski, A., Parinos, C., Dimiza, M., Bouloubassi, I., Luterbacher, J., Kouli, K., Martrat, B., Toreti, A., Fleitmann, D., Rousakis, G., Kaberi, H., Athanasiou, M., Lykousis, V., 2016. Climate variability and socio-environmental changes in the Northern Aegean (NE Mediterranean) during the last 1500 years. Quat. Sci. Rev. 136, 209–228. https://doi.org/10.1016/J.QUASCIREV.2016.01.009.

Goudeau, M.L.S., Reichart, G.J., Wit, J.C., de Nooijer, L.J., Grauel, A.L., Bernasconi, S.M., de Lange, G.J., 2015. Seasonality variations in the central Mediterranean during climate change events in the late holocene. Palaeogeogr. Palaeoclimatol. Palaeoecol. 418, 304–318. https://doi.org/10.1016/J.PALAEO.2014.11.004.

Grauel, A.L., Schmid, T.W., Hu, B., Bergami, C., Capotondi, L., Zhou, L., Bernasconi, S.M., 2013. Calibration and application of the 'clumped isotope' thermometer to foraminifera for high-resolution climate reconstructions. Geochim. Cosmochim. Acta 108, 125–140. https://doi.org/10.1016/J.GCA.2012.12.049.

Grove, A.T., 2001. The 'Little Ice Age' and its geomorphological consequence in Mediterranean Europe. Clim. Chang. 48, 121–136.

Hennekam, R., Jilbert, T., Schnetger, B., De Lange, G.J., 2014. Solar forcing of Nile discharge and sapropel S1 formation in the early to middle holocene eastern Mediterranean. Paleoceanography 29 (5), 343–356. https://doi.org/10.1002/2013PA002553.

Huang, N.E., Shen, Z., Long, S.R., Wu, M.C., Shih, H.H., Zheng, Q., Yen, N.-C., Chao Tung, C., Liu, H.H., 1998. The empirical mode decomposition and the hilbert spectrum for nonlinear and non-stationary time series analysis. Proc. R. Soc. Lond. 454, 903–995.

Incarbona, A., Sprovieri, M., 2020. The postglacial isotopic record of intermediate water connects Mediterranean sapropels and organic-rich layers. Paleoceanogr. Paleoclimatol. 35 (10). https://doi.org/10.1029/2020PA004009.

Incarbona, A., Ziveri, P., Di Stefano, E., Lirer, F., Mortyn, G., Patti, B., Pelosi, N., Sprovieri, M., Tranchida, G., Vallefuoco, M., Albertazzi, S., Bellucci, L., Bonanno, A., Bonomo, S., Censi, P., Ferraro, L., Giuliani, S., Mazzola, S., Sprovieri, R., 2010. Calcareous nannofossil assemblages climate of the past discussions calcareous nannofossil assemblages from the Central Mediterranean Sea over the last four centuries: the impact of the little ice age calcareous nannofossil assemblages. Clim. Past Discuss 6, 817–866. https://doi.org/10.5194/cpd-6-817-2010.

Incarbona, A., Marino, G., Di Stefano, E., Grelaud, M., Pelosi, N., Rodríguez-Sanz, L., Rohling, E.J., 2022. Middle-Late Pleistocene Eastern Mediterranean Nutricline Depth and Coccolith Preservation Linked to Monsoon Activity and Atlantic Meridional Overturning Circulation. https://doi.org/10.1016/j.gloplacha.2022.103946.

Incarbona, A., Bonomo, S., Cacho, I., Lirer, F., Margaritelli, G., Pecoraro, D., Ziveri, P., 2023. Solar forcing for nutricline depth variability inferred by coccoliths in the pre-industrial northwestern Mediterranean. Glob. Planet. Chang. 224, 104102. https://doi.org/10.1016/j.gloplacha.2023.104102.

Jalut, G., Dedoubat, J.J., Fontugne, M., Otto, T., 2009. Holocene circum-Mediterranean vegetation changes: climate forcing and human impact. Quat. Int. 200 (1–2), 4–18. https://doi.org/10.1016/J.QUAINT.2008.03.012.

Jolly, D., Harrison, S.P., Damnati, B., Bonnefille, R., 1998. Simulated climate and biomes of Africa during the late quaternary: comparison with Pollen and Lake Status Data. Quat. Sci. Rev. 17 (6–7), 629–657. https://doi.org/10.1016/S0277-3791(98)00015-8.

Jordan, R.W., Cros, L., Young, J.R., 2004. A revised classification scheme for living haptophytes. Micropaleontology 50 (1), 55–79.

Juggins, S., . Rioja: Analysis of Quaternary Science Data. https://eprints.ncl.ac.uk. Newcastle University.

Kalimeris, A., Ranieri, E., Founda, D., Norrant, C., 2017. Variability modes of precipitation along a central Mediterranean Area and their relations with ENSO, NAO, and other climatic patterns. Atmos. Res. 198, 56–80. https://doi.org/10.1016/J.ATMOSRES.2017.07.031.

Kaplan, J.O., Krumhardt, K.M., Zimmermann, N., 2009. The prehistoric and preindustrial deforestation of Europe. Quat. Sci. Rev. 28 (27–28), 3016–3034.

Karatsolis, B., Th, M.V., Triantaphyllou, M.D., Dimiza, E., Malinverno, A., Lagaria, P., Mara, O.A., Psarra, S., 2017. Coccolithophore assemblage response to Black Sea water inflow into the North Aegean Sea (NE Mediterranean). Cont. Shelf Res. 149, 138–150. https://doi.org/10.1016/J.CSR.2016.12.005.

Kleijne, A., 1991. Holococcolithophorids from the Indian Ocean, Red Sea, Mediterranean Sea and North Atlantic Ocean. Mar. Micropaleontol. 17 (1–2), 1–76. https://doi.org/10.1016/0377-8398(91)90023-Y.

Knappertsbusch, M., 1993. Geographic distribution of living and Holocene coccolithophores in the Mediterranean Sea. Mar. Micropaleontol. 21 (1–3), 219–247. https://doi.org/10.1016/0377-8398(93)90016-Q.

Kobashi, T., Menviel, L., Jeltsch-Thömmes, A., Vinther, B.M., Box, J.E., Muscheler, R., Nakaegawa, T., Pfister, P., Doring, M., Leuenberger, M., Wanner, H., Ohmura, A., 2017. Volcanic influence on centennial to millennial holocene Greenland temperature change. Sci. Rep. 7 (1), 1–10. https://doi.org/10.1038/s41598-017-01451-7.

Kotthoff, U., Groeneveld, J., Ash, J.L., Fanget, A.S., Krupinski, N.Q., Peyron, O., Stepanova, A., Warnock, J., Van Helmond, P., Passey, B., Clausen, O., Bennike, O., Andren, E., Granoszewski, W., Andrén, T., Filipsson, H., Seidenkrantz, M., Slomp, C., Bauersachs, T., 2017. Reconstructing holocene temperature and salinity variations in the western baltic sea region: a multi-proxy comparison from the little belt (IODP Expedition 347, Site M0059). Biogeosciences 14 (23), 5607–5632. https://doi.org/10.5194/BG-14-5607-2017.

Lambeck, K., Rouby, H., Purcell, A., Sun, Y., Sambridge, M., 2014. Sea level and global ice volumes from the last glacial maximum to the holocene. Proc. Natl. Acad. Sci. USA 111 (43), 15296–15303. https://doi.org/10.1073/PNAS.1411762111.

Lavigne, H., Civitarese, G., Gacie, M., D'Ortenzio, F., 2018. Impact of decadal reversals of the north ionian circulation on phytoplankton phenology. Biogeosciences 15 (14), 4431–4445. https://doi.org/10.5194/bg-15-4431-2018.

Le Houedec, S., Mojtahid, M., Bicchi, E., de Lange, G.J., Hennekam, R., 2020. Suborbital hydrological variability inferred from coupled benthic and planktic foraminiferal-based proxies in the Southeastern Mediterranean during the last 19 Ka. Paleoceanogr. Paleoclimatol. 35 (2), e2019PA003827. https://doi.org/10.1029/2019PA003827.

Lechleitner, F.A., Breitenbach, S.F.M., Cheng, H., Plessen, B., Rehfeld, K., Goswami, B., Marwan, N., Eroglu, D., Adkins, J., Huad, G., 2017. Climatic and in-cave influences on $\delta^{18}O$ and $\delta^{13}C$ in a stalagmite from northeastern India through the last deglaciation. Quat. Res. 88 (3), 458–471. https://doi.org/10.1017/qua.2017.72.

Leng, M., Barker, P., Greenwood, P., Roberts, N., Reed, J., 2001. Oxygen isotope analysis of diatom silica and authigenic calcite from Lake Pinarbasi, Turkey. J. Paleolimnol. 25.

Lirer, F., Sprovieri, M., Vallefuoco, M., Ferraro, L., Pelosi, N., Giordano, L., Capotondi, L., 2014. Planktonic foraminifera as bio-indicators for monitoring the climatic changes that have occurred over the past 2000 years in the Southeastern Tyrrhenian Sea. Integr. Zool. 9 (4), 542–554. https://doi.org/10.1111/1749-4877.12083.

Lirer, F., Foresi, L.M., Iaccarino, S.M., Salvatorini, G., Turco, E., Cosentino, C., Sierro, F. J., Caruso, A., 2019. Mediterranean neogene planktonic foraminifer biozonation and biochronology. Earth Sci. Rev. 196, 102869. https://doi.org/10.1016/J.EARSCIREV.2019.05.013.

López-Moreno, J.I., Vicente-Serrano, S.M., Morán-Tejeda, E., Lorenzo-Lacruz, J., Kenawy, A., Beniston, M., 2011. Effects of the North Atlantic Oscillation (NAO) on combined temperature and precipitation winter modes in the Mediterranean Mountains: observed relationships and projections for the 21st century. Glob. Planet. Chang. 77 (1–2), 62–76. https://doi.org/10.1016/J.GLOPLACHA.2011.03.003.

Lüning, S., Schulte, L., Garcés-Pastor, S., Danladi, I.B., M., Gałka., 2019. The medieval climate anomaly in the Mediterranean Region. Paleoceanogr. Paleoclimatol. 34 (10), 1625–1649. https://doi.org/10.1029/2019PA003734.

Luukko, P.J.J., Helske, J., Räsänen, E., 2016. Introducing libeemd: a program package for performing the ensemble empirical mode decomposition. Comput. Stat. 31 (2), 545–557. https://doi.org/10.1007/S00180-015-0603-9/FIGURES/4.

Mackensen, A., Schmiedl, G., 2019. Stable carbon isotopes in paleoceanography: atmosphere, oceans, and sediments. Earth Sci. Rev. 197, 102893. https://doi.org/10.1016/j.earscirev.2019.102893.

Magny, M., Miramont, C., Sivan, O., 2002. Assessment of the impact of climate and anthropogenic factors on holocene Mediterranean vegetation in Europe on the basis of palaeohydrological records. Palaeogeogr. Palaeoclimatol. Palaeoecol. 186 (1–2), 47–59. https://doi.org/10.1016/S0031-0182(02)00442-X.

Magny, M., Combourieu-Nebout, N., De Beaulieu, J.L., Bout-Roumazeilles, V., Colombaroli, D., Desprat, S., Francke, A., Joannin, S., Ortu, E., Peyron, O., Revel, M., Sadori, L., Siani, G., Sicre, M., Samartin, S., Simonneau, A., Tinner, W., Vannière, B., Wagner, B., Zanchetta, G., Anselmetti, F., Brugiapaglia, E., Chapron, E., Debret, M., Desmet, M., Didier, J., Essallami, L., Galop, D., Gilli, A., Haas, J., Kallel, N., Millet, L., Stock, A., Turon, J., Wirth, S., 2013. North-South palaeohydrological contrasts in the Central Mediterranean during the holocene: tentative synthesis and working hypotheses. Clim. Past 9 (5), 2043–2071. https://doi.org/10.5194/cp-9-2043-2013.

Malinverno, E., Ziveri, P., Corselli, C., 2003. Coccolithophorid distribution in the Ionian Sea and its relationship to eastern Mediterranean circulation during late fall to early winter 1997. J. Geophys. Res. 108 (C9). https://doi.org/10.1029/2002JC001346.

Malinverno, E., Triantaphyllou, M.V., Stavrakakis, S., Ziveri, P., Lykousis, V., 2009. Seasonal and spatial variability of coccolithophore export production at the South-Western Margin of Crete (Eastern Mediterranean). Mar. Micropaleontol. 71 (3–4), 131–147. https://doi.org/10.1016/J.MARMICRO.2009.02.002.

Malinverno, E., Maffioli, P., Corselli, C., De Lange, G.J., 2014. Present-day fluxes of coccolithophores and diatoms in the pelagic Ionian Sea. J. Mar. Syst. 132, 13–27. https://doi.org/10.1016/j.jmarsys.2013.12.009.

Mallo, M., Ziveri, P., Mortyn, P.G., Schiebel, R., Grelaud, M., 2017. Low planktic foraminiferal diversity and abundance observed in a spring 2013 west-East Mediterranean Sea plankton tow transect. Biogeosciences 14, 2245–2266.

Manca, B.B., Budillon, G., Scarazzato, P., Ursella, L., 2003. Evolution of dynamics in the eastern Mediterranean affecting water mass structures and properties in the Ionian and Adriatic Seas. J. Geophys. Res. 108 (9). https://doi.org/10.1029/2002jc001664.
Margaritelli, G., Vallefuoco, M., Di Rita, F., Capotondi, L., Bellucci, L.G., Insinga, D.D., Petrosino, P., Bonomo, S., Cacho, I., Cascella, A., Ferraro, L., Florindo, F., Lubritto, C., Lurcock, P., Magri, D., Pelosi, N., Rettori, R., Lirer, F., 2016. Marine Response to climate changes during the last five Millennia in the Central Mediterranean Sea. Glob. Planet. Chang. 142, 53–72. https://doi.org/10.1016/J.GLOPLACHA.2016.04.007.
Margaritelli, G., Cisneros, M., Cacho, I., Capotondi, L., Vallefuoco, M., Rettori, R., Lirer, F., 2018. Climatic variability over the last 3000 years in the Central - Western Mediterranean Sea (Menorca Basin) detected by planktonic foraminifera and stable isotope records. Glob. Planet. Chang. 169, 179–187. https://doi.org/10.1016/J.GLOPLACHA.2018.07.012.
Margaritelli, G., Cacho, I., Català, A., Barra, M., Bellucci, L.G., Lubritto, C., Rettori, R., Lirer, F., 2020. Persistent warm Mediterranean surface waters during the Roman Period. Sci. Rep. 10 (1), 1–10. https://doi.org/10.1038/s41598-020-67281-2.
Margaritelli, G., Lirer, F., Schroeder, K., Cloke-Hayes, A., Caruso, A., Capotondi, L., Broggy, T., Cacho, I., Sierro, F.J., 2022. *Globorotalia truncatulinoides* in the Mediterranean Basin during the middle-late holocene: bio-chronological and oceanographic indicator. Geosciences 12 (6). https://doi.org/10.3390/geosciences12060244.
Marino, M., Maiorano, P., Lirer, F., Pelosi, N., 2009. Response of calcareous nannofossil assemblages to paleoenvironmental changes through the mid-pleistocene revolution at site 1090 (Southern Ocean). Palaeogeogr. Palaeoclimatol. Palaeoecol. 280 (3–4), 333–349. https://doi.org/10.1016/J.PALAEO.2009.06.019.
Marshall, J., Kushnir, Y., Battisti, D., Chang, P., Czaja, A., Dickson, R., Hurrell, J., McVartney, M., Saravanan, R., Visbeck, M., 2002. North Atlantic climate variability: phenomena, impacts and mechanisms. Int. J. Climatol. 21, 1863–1898. https://doi.org/10.1002/joc.693.
Martinez-Ruiz, F., Kastner, M., Gallego-Torres, D., Rodrigo-Gámiz, M., Nieto-Moreno, V., Ortega-Huertas, M., 2015. Paleoclimate and paleoceanography over the past 20,000yr in the Mediterranean Sea basins as indicated by sediment elemental proxies. Quat. Sci. Rev. https://doi.org/10.1016/j.quascirev.2014.09.018.
Martinez-Ruiz, F., Kastner, M., Paytan, A., Ortega-Huertas, M., Bernasconi, S.M., 2000. Geochemical evidence for enhanced productivity during S1 sapropel deposition in the easrern Mediterranean. Paleoc. 15 (2), 200–209. https://doi.org/10.1029/1999PA000419.
Mayewski, P.A., Rohling, E.E., Stager, J.C., Karlén, W., Maasch, K.A., Meeker, L.D., Meyerson, E.A., Gasse, F., van Kreveld, S., Holmgren, K., Lee-Thorp, J., Rosqvist, G., Rack, F., Staubwasser, M., Schneider, R., Steig, E., 2004. Holocene climate variability. Quat. Res. 62 (3), 243–255. https://doi.org/10.1016/J.YQRES.2004.07.001.
Meier, K.S., Zonneveld, K.A., Kasten, S., H., Willems., 2004. Different nutrient sources forcing increased productivity during eastern Mediterranean S1 sapropel formation as reflected by calcareous dinoflagellate cysts. Paleoceanography 19 (1).
Mensing, S., Tunno, I., Cifani, G., Passigli, S., Noble, P., Archer, C., G., Piovesan., 2016. Human and climatically induced environmental change in the Mediterranean during the medieval climate Anomaly and Little Ice Age: a case from Central Italy. Anthropocene 15, 49–59. https://doi.org/10.1016/J.ANCENE.2016.01.003.
Milligan, T.G., Cattaneo, A., 2007. Sediment dynamics in the western Adriatic Sea: from transport to stratigraphy. Cont. Shelf Res. 27 (3–4), 287–295. https://doi.org/10.1016/J.CSR.2006.11.001.
Molcard, A., Pinardi, N., Iskandarani, M., Haidvogel, D.B., 2002. Wind driven general circulation of the Mediterranean Sea simulated with a spectral element ocean model. Dyn. Atmos. Oceans 35 (2), 97–130. https://doi.org/10.1016/S0377-0265(01)00080-X.
Morellon, M., Valero-Garcés, B., Gonzalez-Samperiz, P., Vegas-Vilarrubia, T., Rubio, E., Rieradevall, M., Delgado-Huertas, A., Mata, P., Romero, O., Engstrom, D.R., Lopez-Vicente, M., Navas, A., Soto, J., 2009. Climate changes and huma activities recorded in the sediments of Lake Estanya (NE Spain) during the Medieval Warm Period and Little Ice Age. J. Paleolimnol. 46, 423–425. https://doi.org/10.1007/s10933-009-9346-3.
Muhs, D.R., 2013. The geologic records of dust in the Quaternary. Aeolian Res. 9, 3–48.
Mulitza, S.H., Arz, S. Kemle-von, Mucke, C., Moos, H.-S., Niebler, J. Patzold, Segl, M., 1999. The South Atlantic carbon isotope record of planktic foraminifera. In: Fischer, G., Wefer, G. (Eds.), Use of Proxies in Paleoceanography. Springer, Berlin, Heidelberg. https://doi.org/10.1007/978-3-642-58646-0_17.
Negri, A., Giunta, S., 2001. Calcareous nannofossil paleoecology in the sapropel S1 of the Eastern Ionian Sea: paleoceanographic implications. Palaeogeogr. Palaeoclimatol. Palaeoecol. 169 (1–2), 101–112. https://doi.org/10.1016/S0031-0182(01)00219-X.
Negri, A., Capotondi, L., Keller, J., 1999. Calcareous nannofossils, planktonic foraminifera and oxygen isotopes in the late quaternary sapropels of the Ionian Sea. Mar. Geol. 157, 89–103. https://doi.org/10.1016/S0025-3227(98)00135-2.
Nicault, A., Alleaume, S., Brewer, S., Carrer, Marco, Nola, P., Guiot, J., 2008. Mediterranean drought fluctuation during the last 500 years based on tree-ring data. Clim. Dyn. 31 (2–3), 227–245. https://doi.org/10.1007/S00382-007-0349-3/FIGURES/9.
Nieto-Moreno, V., Martínez-Ruiz, F., Giralt, S., Jiménez-Espejo, F., Gallego-Torres, D., Rodrigo-Gámiz, M., García-Orellana, J., Ortega-Huertas, M., De Lange, G.J., 2011. Tracking climate variability in the Western Mediterranean during the late Holocene: a multiproxy approach. Clim. Past 7 (4), 1395–1414. https://doi.org/10.5194/CP-7-1395-2011.
O'Brien, S.R., Mayewski, P.A., Meeker, L.D., Meese, D.A., Twickler, M.S., Whitlow, S.I., 1995. Complexity of Holocene climate as reconstructed from a greenland ice core. Science 270 (5244), 1962–1964. https://doi.org/10.1126/SCIENCE.270.5244.1962.
Okada, H., McIntyre, A., 1977. Modern coccolithophores of the Pacific and North Atlantic Oceans. Micropaleontology 23 (1), 1. https://doi.org/10.2307/1485309.
Olsen, J., Kjær, K.H., Funder, S., Larsen, N.K., Ludikova, A., 2012. High-Arctic climate conditions for the last 7000 years inferred from multi-proxy analysis of the Bliss Lake record, North Greenland. J. Quat. Sci. 27, 318–327. https://doi.org/10.1002/jqs.1548.
Oviedo, A., Ziveri, P., Álvarez, M., Tanhua, T., 2015. Is coccolithophore distribution in the Mediterranean Sea related to seawater carbonate chemistry? Ocean Sci. 11 (1), 13–32. https://doi.org/10.5194/OS-11-13-2015.
Özsoy, E., Hecht, A., Ünlüata, Ü., 1989. Circulation and hydrography of the Levantine Basin. Results of POEM coordinated experiments 1985–1986. Prog. Oceanogr. 22 (2), 125–170. https://doi.org/10.1016/0079-6611(89)90004-9.
Persoiu, A., Ionita, M., Weiss, H., 2019. Atmospheric blocking induced by the strengthened siberian high led to drying in West Asia during the 4.2 Ka BP event-a hypothesis. Clim. Past 15 (2), 781–793. https://doi.org/10.5194/cp-15-781-2019.
Peyron, O., Goring, S., Dormoy, I., Kotthoff, U., Pross, J., de Beaulieu, J.L., Drescher-Schneider, R., Vanniére, B., Magny, M., 2011. Holocene seasonality changes in the Central Mediterranean region reconstructed from the pollen sequences of Lake Accesa (Italy) and Tenaghi Philippon (Greece). The Holocene 21 (1), 131–146. https://doi.org/10.1177/0959683610384162.
Peyron, O., Combourieu-Nebout, N., Brayshaw, D., Goring, S., Andrieu-Ponel, V., Desprat, S., Fletcher, W., Gambin, B., Ioakim, C., Joannin, S., Kotthoff, U., Kouli, K., Montade, V., Pross, J., Sadori, L., Magny, M., 2017. Precipitation changes in the Mediterranean Basin during the Holocene from terrestrial and marine pollen records: a model-data comparison. Clim. Past 13 (3), 249–265. https://doi.org/10.5194/cp-13-249-2017.
Piccarreta, M., Caldara, M., Capolongo, D., Boenzi, F., 2011. Holocene geomorphic activity related to climatic change and human impact in Basilicata, Southern Italy. Geomorphology 128 (3–4), 137–147. https://doi.org/10.1016/J.GEOMORPH.2010.12.029.
Pinardi, N., Zavatarelli, M., Adani, M., Coppini, G., Fratianni, C., Oddo, P., Simoncelli, S., Tonani, M., Lyubartsev, V., Dobricic, S., Bonaduce, A., 2015. Mediterranean Sea large-scale low-frequency ocean variability and water mass formation rates from 1987 to 2007: a retrospective analysis. Prog. Oceanogr. https://doi.org/10.1016/j.pocean.2013.11.003.
Piva, A., Asioli, A., Trincardi, F., Schneider, R.R., Vigliotti, L., 2008. Late-Holocene climate variability in the Adriatic Sea (Central Mediterranean). Holocene 18 (1), 153–167. https://doi.org/10.1177/0959683607085606.
Principato, M.S., Giunta, S., Corselli, C., Negri, A., 2003. Late Pleistocene-Holocene planktonic assemblages in three box-cores from the Mediterranean Ridge area (west-southwest of Crete): palaeoecological and palaeoceanographic reconstruction sapropel S1 interval. Palaeogeogr. Palaeoclimatol. Palaeoecol. 190, 61–77. https://doi.org/10.1016/S0031-0182(02)00599-0.
Pujol, C., Vergnaud Grazzini, C., 1995. Distribution patterns of live planktic foraminifers as related to regional hydrography and productive systems of the Mediterranean Sea. Mar. Micropaleontol. 25 (2–3), 187–217. https://doi.org/10.1016/0377-8398(95)00002-I.
Richter, T.O., Van Der Gaast, S., Koster, B., Vaars, A., Gieles, R., De Stigter, H.C., De Haas, H., Van Weering, T.C.E., 2006. The avaatech XRF core scanner: technical description and applications to NE Atlantic sediments. Geol. Soc. Spec. Publ. 267, 39–50. https://doi.org/10.1144/GSL.SP.2006.267.01.03.
Rigual-Hernández, A.S., Sierro, F.J., Bárcena, M.A., Flores, J.-A., Heussner, S., 2012. Seasonal and interannual changes of planktic foraminiferal fluxes in the Gulf of Lions (NW Mediterranean) and their implications for paleoceanographic studies: two 12-year sediment trap records. Deep Sea Res. Part 1 Oceanogr. Res. Pap. 66, 26–40. https://doi.org/10.1016/j.dsr.2012.03.011.
Rincón-Martínez, D., Lamy, F., Contreras, S., Leduc, G., Bard, E., Saukel, C., Blanz, T., MacKensen, A., Tiedemann, R., 2010. More humid interglacials in Ecuador during the past 500 Kyr linked to latitudinal shifts of the equatorial front and the intertropical convergence zone in the Eastern Tropical Pacific. Paleoceanography 25 (2). https://doi.org/10.1029/2009PA001868.
Rio, D., Raffi, I., Villa, G., 1990. Pliocene-pleistocene calcareous nannofossil distribution parrerns in the western Mediterranean. Proc. Ocean Drill. Progr. Sci. Res. 533107 (107), 513–533.
Ritchie, J.C., Eyles, C.H., Haynes, C.V., 1985. Sediment and pollen evidence for an early to mid-holocene humid period in the Eastern Sahara. Nature 314 (6009), 352–355. https://doi.org/10.1038/314352a0.
Roberts, N., Eastwood, W.J., Kuzucuoğlu, C., Fiorentino, G., Caracuta, V., 2011. Climatic, vegetation and cultural change in the eastern Mediterranean during the mid-holocene environmental transition. Holocene 21 (1), 147–162. https://doi.org/10.1177/0959683610386819.
Roesch, A., Schmidbauer, H., 2018. Computational Wavelet Analysis. https://www.researchgate.net/profile/Harald-Schmidbauer/publication/323836523_WaveletComp_11_A_guided_tour_through_the_R_package/links/5abbc0f0aca27222c7536677/WaveletComp-11-A-guided-tour-through-the-R-package.pdf.
Rohling, E.J., 1994. Review and new aspects concerning the formation of eastern Mediterranean sapropels. Mar. Geol. 122 (1–2), 1–28.
Rohling, E.J., 2000. Paleosalinity: confidence limits and future applications. Mar. Geol. 163 (1–4), 1–11. https://doi.org/10.1016/S0025-3227(99)00097-3.
Rohling, E.J., Cooke, S., 1999. Stable oxygen and carbon isotopes in foraminiferal carbonate shells. In: Sen Gupta, B.K. (Ed.), Modern Foraminifera. Kluwer Academic Publishers, Dordrecht/Boston/London, pp. 239–258.
Rohling, E.J., De Rijk, S., 1999. Holocene climate optimum and last glacial maximum in the Mediterranean: the marine oxygen isotope record. Mar. Geol. 153 (1–4), 57–75. https://doi.org/10.1016/S0025-3227(98)00020-6.

Rohling, E.J., Den Dulk, M., Pujol, C., Vergnaud-Grazzini, C., 1995. Abrupt hydrographic change in the Alboran Sea (Western Mediterranean) around 8000 Yrs BP. Deep-Sea Res. I Oceanogr. Res. Pap. 42 (9), 1609–1619. https://doi.org/10.1016/0967-0637(95)00069-I.

Rohling, E., Mayewski, P., Abu-Zied, R., Casford, J., Hayes, A., 2002. Holocene atmosphere-ocean interactions: records from Greenland and the Aegean Sea. Clim. Dyn. 18 (7), 587–594. https://doi.org/10.1007/s00382-001-0194-8.

Rohling, E.J., Sprovieri, M., Cane, T., Casford, J.S.L., Cooke, S., Bouloubassi, I., Emeis, K. C., Schiebel, R., Rogerson, M., Hayes, A., Jorissen, F.J., Kroon, D., 2004. Reconstructing planktic foraminiferal habitats using stable isotope data: a case history for Mediterranean sapropel S5. Mar. Micropaleontol. 50 (1), 89–123.

Rohling, E. J., K. Grant, M. Bolshaw, A. P. Roberts, M. Siddall, Ch Hemleben, and M. Kucera. 2009. "Antarctic temperature and global sea level closely coupled over the past five glacial cycles." *Nat. Geosci. 2*(7). 500–504. doi:https://doi.org/10.1038/ngeo557.

Rohling, E.J., Marino, G., Grant, K.M., 2015. Mediterranean climate and oceanography, and the periodic development of anoxic events (Sapropels). Earth Sci. Rev. https://doi.org/10.1016/j.earscirev.2015.01.008.

Rossi, V., Vaiani, S.C., 2008. Benthic foraminiferal evidence of sediment supply changes and fluvial drainage reorganization in Holocene deposits of the Po delta, Italy. Mar. Micropaleontol. 69 (2), 106–118. https://doi.org/10.1016/j.marmicro.2008.07.001.

Rossignol-Strick, M., Nesteroff, W., Olive, P., Vergnaud Grazzini, C., 1982. After the deluge: Mediterranean stagnation and sapropel formation. Nature 295 (5845), 105–110. https://doi.org/10.1038/295105a0.

Roth, P., 1994. Distribution of coccoliths in ocean sediments. In: Winter, A., Siesser, W.G. (Eds.), Volume Coccolithophores. Cambridge University Press, pp. 199–218.

Roth, P.H., Coulbourn, W.T., 1982. Floral and solution patterns of coccoliths in surface sediments of the North Pacific. Mar. Micropaleontol. 7 (1), 1–52. https://doi.org/10.1016/0377-8398(82)90014-7.

Rothwell, R.G., Rack, F.R., 2006. New techniques in sediment core analysis: an introduction. Geol. Soc. Spec. Publ. 267, 1–29. https://doi.org/10.1144/GSL.SP.2006.267.01.01.

Sadori, L., Zanchetta, G., Giardini, M., 2008. Last glacial to holocene palaeoenvironmental evolution at Lago Di Pergusa (Sicily, Southern Italy) as inferred by pollen, microcharcoal, and stable isotopes. Quat. Int. 181 (1), 4–14. https://doi.org/10.1016/J.QUAINT.2007.02.024.

Sangiorgi, F., Capotondi, L., Combourieu Nebout, N., Vigliotti, L., Brinkhuis, H., Giunta, S., Lotter, A.F., Morigi, C., Negri, A., Reichart, G.-J., 2003. Holocene seasonal sea-surface temperature variations in the southern Adriatic Sea inferred from a multiproxy approach. J. Quat. Res. 18 (8), 723–732. https://doi.org/10.1002/JQS.782.

Shindell, D.T., Schmidt, G.A., Miller, R.L., Mann, M.E., 2003. Volcanic and Solar Forcing of climate Change during the Preindustrial Era. J. Clim. 16, 4094–4107.

Shindell, D.T., Faluvegi, G., Schmidt, G.A., 2020. Influences of solar forcing at ultraviolet and longer wavelengths on climate. J. Geophys. Res.-Atmos. 125 (7). https://doi.org/10.1029/2019JD031640.

Siani, G., Paterne, M., C., Colin., 2010. Late glacial to Holocene planktic foraminifera bioevents and climatic record in the South Adriatic Sea. J. Quat. Sci. 25 (5), 808–821.

Siani, G., Magny, M., Paterne, M., Debret, M., Fontugne, M., 2013. Paleohydrology reconstruction and holocene climate variability in the South Adriatic Sea. Clim. Past 9 (1), 499–515. https://doi.org/10.5194/cp-9-499-2013.

Skampa, E., Triantaphyllou, M.V., Dimiza, M.D., Gogou, A., Malinverno, E., Stavrakakis, S., Panagiotopoulos, I.P., Parinos, C., Baumann, K.H., 2019. Coupling plankton - sediment trap - surface sediment coccolithophore regime in the North Aegean Sea (NE Mediterranean). Mar. Micropaleontol. 152, 101729. https://doi.org/10.1016/J.MARMICRO.2019.03.001.

Skampa, E., Triantaphyllou, M.V., Dimiza, M.D., Gogou, A., Malinverno, E., Stavrakakis, S., Parinos, C., Panagiotopoulos, I., Tselenti, D., Archontikis, O., Baumann, K.-H., 2020. Coccolithophore export in three deep-sea sites of the Aegean and Ionian Seas (Eastern Mediterranean): biogeographical patterns and biogenic carbonate fluxes. Deep Sea Res. II 171, 104690. https://doi.org/10.1016/J.DSR2.2019.104690.

Skampa, E., Dimiza, M.D., Arabas, A., Gogou, A., Panagiotopoulos, I.P., Tsourou, T., Velaoras, D., Karagiorgas, M., Baumann, K.-H., Triantaphyllou, M.V., 2024. The Cretan Basin (South Aegean Sea, NE Mediterranean) in the early Pliocene: a paleoceanographic reconstruction. Palaeogeogr. Palaeoclimatol. Palaeoecol. 640, 112085. https://doi.org/10.1016/j.palaeo.2024.112085.

Skonieczny, C., Paillou, P., Bory, A., Bayon, G., Biscara, L., Crosta, X., Eynaud, F., Malaizé, B., Revel, M., Aleman, N., Barusseau, J.-P., Vernet, R., Lopez, S., Grousset, F., 2015. African humid periods triggered the reactivation of a large river system in Western Sahara. Nat. Commun. 6, 8751. https://doi.org/10.1038/ncomms9751.

Smith, A.C., Wynn, P.M., Barker, P.A., Leng, M.J., Noble, S.R., Tych, W., 2016. North Atlantic forcing of moisture delivery to Europe throughout the Holocene. Sci. Rep. 6 (1), 1–7. https://doi.org/10.1038/srep24745.

Solanki, S.K., Usoskin, I.G., Kromer, B., Schüssler, M., Beer, J., 2004. Unusual activity of the Sun during recent decades compared to the previous 11,000 years. Nature 431, 1084–1087. https://doi.org/10.1038/NATURE02995.

Solignac, S., Solveig Seidenkrantz, M., Jessen, C., Kuijpers, A., Gunvald, A.K., Olsen, J., 2011. Late-holocene sea-surface conditions offshore newfoundland based on dinoflagellate cysts. Holocene 21 (4), 539–552. https://doi.org/10.1177/0959683610385720.

Sorrel, P., Debret, M., Billeaud, I., Jaccard, S.L., McManus, J.F., Tessier, B., 2012. Persistent non-solar forcing of holocene storm dynamics in coastal sedimentary archives. Nat. Geosci. 5 (12), 892–896. https://doi.org/10.1038/ngeo1619.

Spero, H.J., 1992. Do planktic foraminifera accurately record shifts in the carbon isotopic composition of seawater SCO_2? Mar. Micropaleontol. 19, 275–285.

Sprovieri, R., Di Stefano, E., Incarbona, A., Gargano, M.E., 2003. A high-resolution record of the last deglaciation in the sicily channel based on foraminifera and calcareous nannofossil quantitative distribution. Palaeogeogr. Palaeoclimatol. Palaeoecol. 202 (1–2), 119–142. https://doi.org/10.1016/S0031-0182(03)00632-1.

Tangunan, D., Baumann, K.-H., Pätzold, J., Henrich, R., Kucera, M., De Pol-Holz, R., Groeneveld, J., 2017. Insolation forcing of coccolithophore productivity in the Western Tropical Indian Ocean over the last two glacial-interglacial cycles. Paleoceanography 32 (7), 692–709. https://doi.org/10.1002/2017PA003102.

Tesi, T., Asioli, A., Minisini, D., Maselli, V., Dalla Valle, G., Gamberi, F., Langone, L., Cattaneo, A., Motagna, P., F., Trincardi., 2017. Large-scale response of the Eastern Mediterranean thermohaline circulation to African monsoon intensification during sapropel S1 formation. Quat. Sci. Rev. 159, 139–154.

Thamban, M., Kawahata, H., Rao, V.P., 2007. Indian summer monsoon variability during the Holocene as recorded in sediments of the Arabian Sea: timing and implications. J. Oceanogr. 63 (6), 1009–1020. https://doi.org/10.1007/S10872-007-0084-8/METRICS.

Theocharis, A., Krokos, G., Velaoras, D., Korres, G., 2014. An internal mechanism driving the alternation of the Eastern Mediterranean dense/deep water sources. In: The Mediterranean Sea: Temporal Variability and Spatial Patterns, pp. 113–137. https://doi.org/10.1002/9781118847572.CH8.

Triantaphyllou, M.V., Ziveri, P., Tselepides, A., 2004. Coccolithophore Export Production and Response to Seasonal Surface Water Variability in the Oligotrophic Cretan Sea (NE Mediterranean). Micropaleontology 50 (Suppl_1), 127–144. https://doi.org/10.2113/50.Suppl_1.127.

Triantaphyllou, M.V., Ziveri, P., Gogou, A., Marino, G., Lykousis, V., Bouloubassi, I., Emeis, K.C., Kouli, K., Dimiza, M., Rosell-Melé, A., Papanikolaou, M., Katsouras, G., Nunez, N., 2009. Late glacial–holocene climate variability at the south-eastern margin of the Aegean Sea. Mar. Geol. 266 (1–4), 182–197. https://doi.org/10.1016/J.MARGEO.2009.08.005.

Triantaphyllou, M.V., Gogou, A., Bouloubassi, I., Dimiza, M., Kouli, K., Roussakis, G., Kotthoff, U., Emeis, K.-C., Papanikolaou, M., Athanasiou, M., Parinos, K., Ioakim, C., Lykousis, V., 2014. Evidence for a warm and humid Mid-Holocene episode in the Aegean and northern Levantine Seas (Greece, NE Mediterranean). Reg. Environ. Chang. 14, 1697–1712.

Triantaphyllou, M.V., Gogou, A., Dimiza, M.D., Kostopoulou, S., Parinos, K., Rousakis, G., Geraga, M., Bouloubassi, I., Fleitmann, D., Zervakis, V., Velaoras, D., Diamantopoulou, A., Sampatakaki, A., Lykousis, V., 2016. Holocene climatic optimum decadal-scale paleoceanography in the NE Aegean (Mediterranean Sea). Geo-Mar. Lett. 31, 51–66.

Trias-Navarro, S., Cacho, I., de la Fuente, M., Pena, L.D., Frigola, J., Lirer, F., Caruso, A., 2021. Surface hydrographic changes at the western flank of the Sicily channel associated with the last sapropel. Glob. Planet. Chang. 204, 103582. https://doi.org/10.1016/J.GLOPLACHA.2021.103582.

Trias-Navarro, S., Pena, L.D., de la Fuente, M., Paredes, E., Garcia-Solsona, E., Frigola, J., Català, A., Caruso, A., Lirer, F., Haghipour, N., Pérez-Asensio, J.N., Cacho, I., 2023. Eastern Mediterranean water outflow during the Younger Dryas was twice that of the present day. Commun. Earth Environ. 4 (1), 1–9. https://doi.org/10.1038/s43247-023-00812-7.

Trouet, V., Esper, J., Graham, N.E., Baker, A., Scourse, J.D., Frank, D.C., 2009. Persistent positive North Atlantic oscillation mode dominated the medieval climate anomaly. Science 324, 78–80. https://doi.org/10.1126/science.1166349.

Turchetto, M., Boldrin, A., Langone, L., Miserocchi, S., Tesi, T., Foglini, F., 2007. Particle transport in the Bari Canyon (southern Adriatic Sea). Mar. Geol. 246 (2–4), 231–247. https://doi.org/10.1016/J.MARGEO.2007.02.007.

Tzedakis, P.C., Hughen, K.A., Cacho, I., Harvati, K., 2007. Placing late neanderthals in a climatic context. Nature 449 (7159), 206–208. https://doi.org/10.1038/nature06117.

Tzedakis, P.C., Pälike, H., Roucoux, K.H., de Abreu, L., 2009. Atmospheric methane, Southern European vegetation and low-mid latitude links on orbital and millennial timescales. Earth Planet. Sci. Lett. 277 (3–4), 307–317. https://doi.org/10.1016/J.EPSL.2008.10.027.

Van Geel, B., Raspopov, O.M., Renssen, H., Van der Plicht, J., Dergachev, V.A., Meijer, H. A.J., 1999. The Role of Solar Forcing upon climate Change. Quat. Sci. Rev. 18 (3), 331–338. https://doi.org/10.1016/S0277-3791(98)00088-2.

Vanniére, B., Power, M.J., Roberts, N., Tinner, W., Carrión, J., Magny, M., Bartlein, P., et al., 2011. Circum-Mediterranean fire activity and climate changes during the Mid-Holocene environmental transition (8500-2500 Cal. BP). Holocene 21 (1), 53–73. https://doi.org/10.1177/0959683610384164.

Vermeersch, P.M., 2008. A holocene prehistoric sequence in the Egyptian Red Sea area: the tree shelter. In: Vermeerscch, P.M. (Ed.), Egyptian Prehistoric Monographs, vol. 7.

Vonmoos, M., Beer, J., Muscheler, R., 2006. Large variations in holocene solar activity: constraints from 10Be in the Greenland ice core project ice core. J. Geophys. Res. 111 (A10). https://doi.org/10.1029/2005JA011500.

Wagner, S., Zorita, E., 2005. The influence of volcanic, solar and CO2 forcing on the temperatures in the Dalton minimum (1790–1830): a model study. Clim. Dyn. 25 (2–3), 205–218. https://doi.org/10.1007/S00382-005-0029-0/FIGURES/10.

Walker, M., Johnsen, S., Rasmussen, S.O., Popp, T., Steffensen, J.P., Gibbard, P., Hoek, W., Lowe, J., Andrews, J., Bjorck, S., Cwynar, L., Hugen, K., Kershaw, P., Kromer, B., Litt, T., Lowe, D., Nakagawa, T., Newnham, R., Schwander, J., 2009. Formal definition and dating of the GSSP (Global Stratotype Section and Point) for the base of the holocene using the Greenland NGRIP ice core, and selected auxiliary records. J. Quat. Sci. 24 (1), 3–17. https://doi.org/10.1002/JQS.1227.

Wanner, H., Brönnimann, S., Casty, C., Gyalistras, D., Luterbacher, J., Schmutz, C., Stephenson, D.B., Xoplaki, E., 2001. North Atlantic Oscillation – Concepts And Studies. Surv. Geophys. 22 (4), 321–381. https://doi.org/10.1023/A:1014217317898.

Wanner, H., Solomina, O., Grosjean, M., Ritz, S.P., Jetel, M., 2011. Structure and origin of holocene cold events. Quat. Sci. Rev. 30 (21–22), 3109–3123. https://doi.org/10.1016/J.QUASCIREV.2011.07.010.

Weltje, G.J., Tjanllingii, R., 2008. Calibration of XRF core scanners for quantitative geochemical logging of sediment cores: theory and applications. Earth Planet Sc. Lett. 274, 4238.

Wirth, S.B., Glur, L., Gilli, A., Anselmetti, F.S., 2013. Holocene flood frequency across the Central Alps – solar forcing and evidence for variations in North Atlantic atmospheric circulation. Quat. Sci. Rev. 80, 112–128. https://doi.org/10.1016/J.QUASCIREV.2013.09.002.

Wu, Z., Huang, N.E., 2011. Ensemble empirical mode decomposition: a noise-assisted data analysis method. World Sci. Publ. Company 1 (1), 1–41. https://doi.org/10.1142/S1793536909000047.

Wu, Z., Huang, N.E., Long, S.R., Peng, C.K., 2007. On the trend, detrending, and variability of nonlinear and nonstationary time series. Proc. Natl. Acad. Sci. 104 (38), 14889–14894.

Young, J., Geisen, M., Cros, L., Kleijne, A., Sprengel, C., Probert, I., Østergaard, J., 2003. A guide to extant coccolithophore taxonomy. J. Nannoplank. Res. Spec. 1.

Zanchetta, G., Giraudi, C., Sulpizio, R., Magny, M., Drysdale, R.N., Sadori, L., 2012. Constraining the onset of the holocene 'neoglacial' over the Central Italy using tephra layers. Quat. Res. 78 (2), 236–247. https://doi.org/10.1016/J.YQRES.2012.05.010.

Ziveri, P., Thunell, R.C., 2000. Coccolithophore export production in Guaymas Basin, Gulf of California: response to climate forcing. Deep Sea Res. II 47 (9–11), 2073–2100. https://doi.org/10.1016/S0967-0645(00)00017-5.

Zielhofer, C., Fletcher, W.J., Mischke, S., De Batist, M., Campbell, J.F.E., Joannin, S., Tjallingii, R., El Hamouti, N., Junginger, A., Stele, A., Bussmann, J., Schneider, B., Lauer, T., Spitzer, K., Strupler, M., Brachert, T., Mikdad, A., 2017. Atlantic forcing of Western Mediterranean winter rain minima during the last 12,000 years. Quat. Sci. Rev. 157, 29–51. https://doi.org/10.1016/j.quascirev.2016.11.037.

Ziveri, P., Baumann, K.-H., Bockel, B., Bollmann, J., Young, J.R., 2004. Biogeography of Selected Holocene Coccoliths in the Atlantic Ocean. *Coccolithophores*. Springer, Berlin, Heidelberg, pp. 403–428. https://doi.org/10.1007/978-3-662-06278-4_15.